Influence of the Last Glacial Maximum on New Jersey shelf offshore fresh groundwater reservoirs – investigating the role of geological heterogeneity

Ariel T. Thomas[1], Sönke Reiche[1], Christoph Clauser[1]

[1]1Institute for Applied Geophysics and Geothermal Energy, RWTH Aachen University, Mathieustrasse 30, 52074 Aachen, Germany.

Corresponding author: Ariel T. Thomas (athomas@eonerc.rwth-aachen.de)

Key Points:

- The Pleistocene sealevel lowstand provided sufficient conditions to freshen most of the mid-Miocene sediments on the New Jersey shelf.
- Onshore-offshore connectivity is not required to explain the mid-shelf freshened reservoirs.
- Downward fingering of saltwater via seafloor-connected pathways in the sediment column compartmentalizes the preserved freshwater system.

Abstract

Offshore freshened groundwater reservoirs occur on continental shelves in several regions of the world. Their origins are an active area of research, however, models often rely on simplified geometrical representations of subsurface geology. The New Jersey shelf hosts an extensive multi-layered freshened groundwater system that previous paleo-reconstructions have not reproduced. In this numerical case-study, we aim to characterize the New Jersey shelf system in the context of a geologically representative heterogeneous model. Our model combines sequence stratigraphic interpretation of 2D depth migrated seismic lines and a stochastic facies distribution with petrophysical properties of four boreholes. We employ a stochastic approach to generate both high and low onshore-offshore connectivity scenarios. The study considers a 58 000-year recharge period for the subaerially exposed shelf transect, followed by the marine transgression from 12 000 years ago until today. The results show that the lowstand period drove sufficient freshwater emplacement that can explain most of the present-day observations. The highest rates of recharge occurred during the periods of most rapid sea-level fall. Simulated scenarios indicate that topographically driven flow of meteoric recharge via surface-connected pathways is the key emplacement mechanism. Surviving freshwater systems exhibit lateral variability in salinity due to downward fingering of saline pore fluid. Freshwater preserved from the Last Glacial Maximum may extend up to 100 km from the coastline. The results also suggest that cyclical flushing and re-salinization of shelf sediments during glacial – interglacial cycles is an asymmetrical process, promoting freshwater storage over geological time scales.

Plain Language Summary

Large volumes of freshwater have been found in sediments on continental margins worldwide. On-going research aims to explain their origins and potential resource viability. The area offshore New Jersey on the Central Atlantic coast of North America contains a complex freshwater reservoir system. We conducted simulations incorporating the existing field data to analyze the history of fluids in the subsurface from the last ice-age until today. Over this period, relatively low sea-level allowed previously salty regions of the subsurface to become flushed with freshwater. We examine the factors which influence the speed and extent of this process. The results show that large volumes of freshwater entered the subsurface at distances over 100 km from the current coastline. As the planet warmed and sealevel rose, complex layering of the rocks in the subsurface protected a portion of this freshwater from the salty ocean water. These offshore reservoirs may contain significant amounts of fresh groundwater and we need to improve our understanding of these complex systems.

1 Introduction

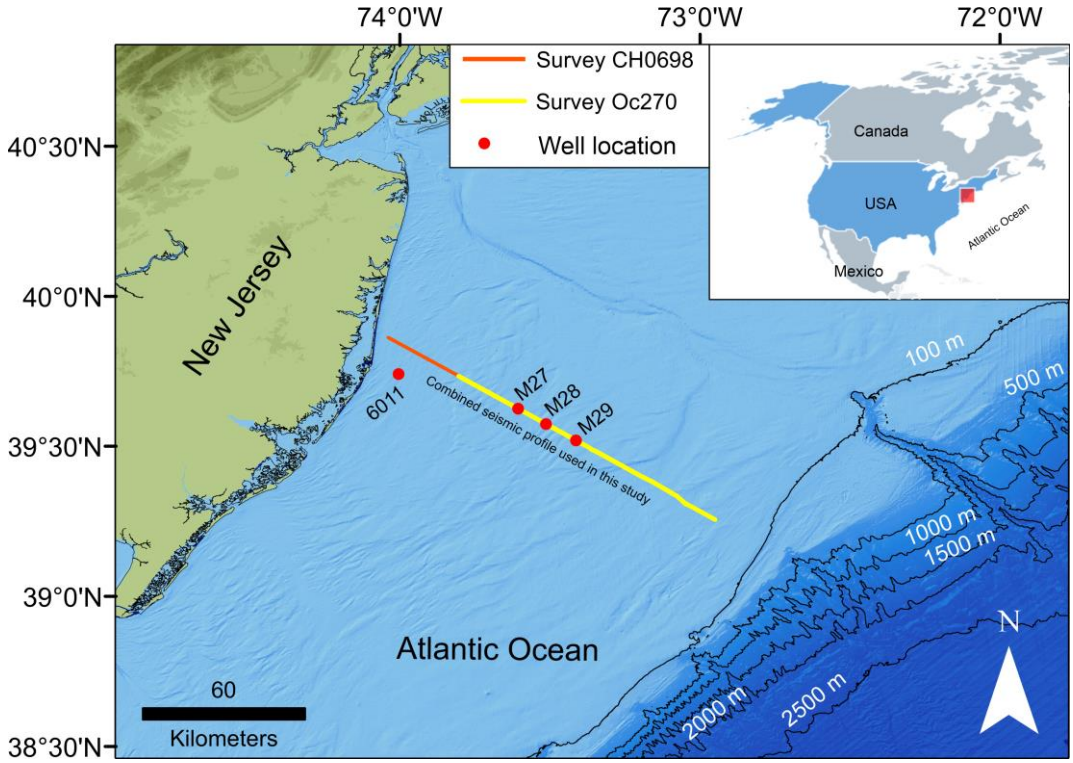

Figure 1 Study location map showing composite seismic line and location of IODP Expedition 313 wells and AMCOR site 6011.

The existence of large reserves of fresh to brackish water in continental shelf sediments has been identified as a global phenomenon (Post et al. 2013). Several studies have investigated these dynamic systems in a number of settings (Groen et al. 2000; Johnston 1983; Lofi et al. 2013; Micallef et al. 2020b), leading to an increased understanding of the key factors that influence the emplacement and survival of offshore fresh groundwater (OFG). A study by Meisler et al. (1984) identified eustatic sea-level changes as a key driver of freshwater emplacement in the New Jersey shelf. Periods of relative sea-level lowstand results in increased hydraulic gradients, driving more freshwater offshore. The sub-aerial exposure of shelf sediments allows for surface recharge by meteoric water. Kooi et al. (2000) performed a numerical study on theoretical shelf models that examined the variety of ways in which emplaced freshwater can be preserved in shelf sediments. The results showed preservation to be a function of the rate of marine transgression as well as the aquifer geometries in the substrate. Glacial – interglacial cycles are known to cause significant sea-level variations and therefore, are fundamentally intertwined with the lifecycle of offshore fresh groundwater. The impact of the Pleistocene glaciation has been examined in regional scale numerical studies on the North American Atlantic margin (Cohen et al. 2010; Siegel et al. 2014). These studies found that the presence of ice-sheet cover contributed significantly to offshore fresh groundwater volumes. It led to increased recharge by subglacial meltwater, and enhanced offshore hydraulic heads due to glacial loading.

The New Jersey shelf sits on the US mid-Atlantic margin, and is considered a classic passive margin setting, with no significant tectonic controls on the sediments. The sedimentary record shows that by the early Oligocene a major shift had occurred from a carbonate ramp deposition to predominantly siliclastic sedimentation (Miller and Snyder 1997). These sediments have been explored by several scientific drilling campaigns. The Atlantic Margin Coring Project (AMCOR) was conducted by the U.S. Geological Survey in 1976. Hathaway et al. (1979) reported that pore fluid studies revealed that much of the Atlantic continental shelf contains fresh – brackish groundwater. Subsequent campaigns include the Ocean Drilling Program legs 150, 150X, 174 and 174X (Austin et al. 1998; Miller et al. 1994); and most recently the International Ocean Discovery Program (IODP) Expedition 313 (Mountain et al. 2010). These later studies were designed to investigate the link between Cenozoic sea-level change and the sedimentary record at the New Jersey shelf. However, pore fluid analysis of core samples by Mountain et al. (2010) revealed multiple layers of fresh – brackish groundwater in the mid-shelf region. The freshwater reservoirs

occur primarily in late Oligocene – Miocene sediments, with low-salinity intervals encountered at depths ranging from just below the seafloor down to 500 m.

Since the initial discovery of extensive offshore freshened groundwater reserves during the AMCOR drilling project (Hathaway et al. 1979), there have been several studies aimed at understanding the hydrogeological evolution of these reservoirs. It was first assumed that the freshwater body was a homogeneous, flat-lying plume, which extended oceanward becoming gradually thinner and more saline. The lens was thought to be fed by submarine groundwater discharge derived from the terrestrial domain. Meisler et al. (1984) conducted a series of simulations on a simple, layered geological model of New Jersey shelf. The study investigated the impact of sea-level, hydraulic conductivity and various permeability anisotropy ratios on the position of a sharp freshwater – seawater interface. Meisler et al. (1984) concluded that the position of the interface was not in equilibrium with present-day sea-level. The authors speculated that freshwater could have been emplaced as early as the Miocene period. Pope and Gordon (1999) investigated the position of the interface on the New Jersey shelf in numerical simulations, implementing sea level variations over a period of 84 000 years. The authors concluded that due to enhanced recharge and discharge of freshwater driven by a fall in sea-level, the oceanward migration of the interface occurs more rapidly relative to the slow-moving rebound when sea-level rises.

A later study analyzing oxygen isotope data by Malone et al. (2002) found that the offshore low-salinity plume was not homogenous, as previously assumed. Oxygen isotope analysis of samples collected in Ocean Drilling Project Leg 174a (Austin et al. 1998) revealed the internal structure of the freshwater distribution in the upper 400 m of the sediment column. The variation was then assumed to be related to high-porosity sand-rich intervals. Pore fluid analysis performed as part of IODP Expedition 313 (sites M27, M28 and M29) revealed a multi-layered reservoir system, with sharp boundaries between fresh and overlying salt water intervals (Mountain et al. 2010). Detailed core analysis by Lofi et al. (2013) revealed that freshwater occurred preferentially in low-permeability intervals, contrary to earlier assumptions. However, this correlation was not ubiquitous. Lofi et al. (2013) presented a new hydrogeological conceptual model of the New Jersey shelf that consisted of multi-layered freshwater reservoirs of varying thickness. Lofi et al. (2013) also suggested that there may be multiple mechanisms of freshwater emplacement responsible for

present day observations. The absolute ages of pore fluid samples from IODP Expedition 313 have not been determined, so the time since these samples have been buried is uncertain. A study by van Geldern et al. (2013) used stable isotope geochemical analysis to argue for a modern meteoric origin of the freshwater. However, the possibility of paleo-groundwater recharge in a period with isotope levels similar to present-day could not be ruled out. Regional numerical studies by Cohen et al. (2010) and Person et al. (2003) identify meteoric recharge during Pleistocene sea-level lowstand as the key source of the freshwater. A resistivity model presented by Gustafson et al. (2019) shows a high-resistivity anomaly, attributed to low salinity pore fluid, which extends landward of the IODP Expedition 313 sites. The authors conclude that the anomaly, obtained by jointly inverting surface-towed controlled source electromagnetic and sea-floor magnetotelluric data, is consistent with land-derived recharge of the offshore freshwater reservoirs.

Research on the origins of the freshwater on the New Jersey shelf has therefore converged around two hypotheses: (1) Fresh groundwater was emplaced during Pleistocene glacial periods, where large parts of the shelf were subaerially exposed. Sea-level lowstand resulted in an increase in the hydraulic head gradient, driving vigorous groundwater flow towards the open sea (Cohen et al. 2010; Hathaway et al. 1979; Person et al. 2003), (2) Offshore fresh groundwater reservoirs are hydraulically connected with onshore aquifers, implying modern recharge by seaward-flowing meteoric groundwater (Gustafson et al. 2019; van Geldern et al. 2013). To date, no study has been conducted on New Jersey samples to determine absolute ages of the freshwater. Previous regional studies did not aim to capture the geological heterogeneity and therefore could not conclusively explain the observed layered distribution. Advances in computing capability have enabled more rigorous testing of larger and increasingly complex hydrogeological models on the Atlantic margin (Cohen et al. 2010; Siegel et al. 2014; Thomas et al. 2019). This has expanded the understanding of mechanisms driving freshwater emplacement and subsequent survival.

The primary focus of this study is to use a geologically heterogeneous shelf model to test the hypothesis that fresh groundwater was emplaced in New Jersey shelf sediments during the period of extended sea-level lowstand associated with the Last Glacial Maximum (LGM). We conducted coupled variable-density flow and heat transport simulations on the 2D shelf transect shown in Figure 1. The shelf model was generated using a workflow originally presented in Thomas et al. (2019). We used a stochastic modelling approach known as Sequential Indicator Simulation (SIS)

to determine a facies distribution, constrained by 2D depth migrated seismic and well data. Porosity and permeability values are assigned to the model domain based on the facies. This approach produces a geologically representative model that captures key characteristics of the sediment heterogeneity and therefore accounts for its influence on the observed salinity distribution. We use a process-based criterion to assess the distribution of flow connectivity in a suite of 100 model realizations. We then selected the two models representing the high- and low onshore-offshore connectivity cases.

We simulated paleo-hydrogeological conditions on the New Jersey transect during the period from the LGM to present day. We consider the past 70 000 years of the hydrogeological evolution of the New Jersey shelf. Firstly, simulations were performed to investigate the sensitivity of the model to key factors that influence offshore freshened groundwater on the continental shelf: (1) topographically driven flow (base case), (2) cemented intervals, (3) enhanced terrestrial discharge and (4) permeability anisotropy. In order to model a meteoric recharge scenario, we consider the specific period of the Pleistocene when the entire surface of the modelled transect was sub-aerially exposed. We determined this recharge phase to be from 70 000 to 12 000 years before present (BP), based on the seafloor bathymetry (Ryan et al. 2009) and sea-level data (Imbrie et al. 1984). The influence of the four factors on the dynamics and distribution of fresh groundwater emplacement on the New Jersey shelf was quantified by comparing the relative volumes of emplaced freshwater at the end of the recharge phase, and at present day. Finally, we simulated the lowstand period considering combinations of the aforementiond driving factors, as plausible reconstructions of hydrogeological scenarios over the past 70 000 years. These simulations allow us to draw conclusions about the evolution of offshore freshened groundwater reservoirs observed in IODP Expedition 313.

We conducted this analysis on a detailed hydrogeological model in order to account for the role of geological heterogeneity in the complex distribution presently observed. These simulations aim to deduce whether meteoric recharge of freshwater on the New Jersey shelf during the last glacial maximum could sufficiently explain present-day observations given a plausible reconstruction of paleo-conditions.

178 # 2 Methodology

179 ## 2.1 Seismic interpretation to hydrogeological model

180 Modelling paleo-groundwater flow on the New Jersey shelf poses the challenge of characterizing
181 the distribution of petrophysical properties in a domain with limited well control. In this study, we
182 generate a facies distribution model utilizing the workflow originally presented in detail by
183 Thomas et al. (2019). The approach combines seismic interpretation with well log analysis to
184 constrain a sequential indicator simulation algorithm. The seismic interpretation presented in
185 Thomas et al. (2019) was extended to include the most landward extensions of the sequences that
186 have been imaged by seismic data. Depth migrated 2D seismic lines are used to constrain the
187 sequence stratigraphic boundaries (Riedel et al. 2018). The profiles include CH068-19 (R/V Cape
188 Hatteras expedition 0698) and OC 270 lines 529, 129-429 and 29 (R/V Oceanus expedition
189 OC270). The nomenclature for the interpreted Miocene sequences were defined after Miller et al.
190 (2013). The extended interpretation is shown in Figure 2.

191 The model domain is centered on adjacent 2D seismic lines which extend 161 km from the coast
192 to close to the shelf edge. The interpretation shown in Figure 2 consists of 25 horizons, from the
193 ocean floor to the lowermost sequence boundary o1, identified as the Eocene-Oligocene boundary
194 (Miller et al. 2013). This basal sequence is the deepest horizon for which a coherent seismic event
195 could be identified. Below this surface, homogeneous model properties were assigned. The 2D
196 model domain has dimensions of 161 km x 2 km and is discretized on a finite difference grid. Cell
197 dimensions are constant throughout the model domain at 100 m in the horizontal and 10 m in the
198 vertical. The entire model comprises 322 000 cells.

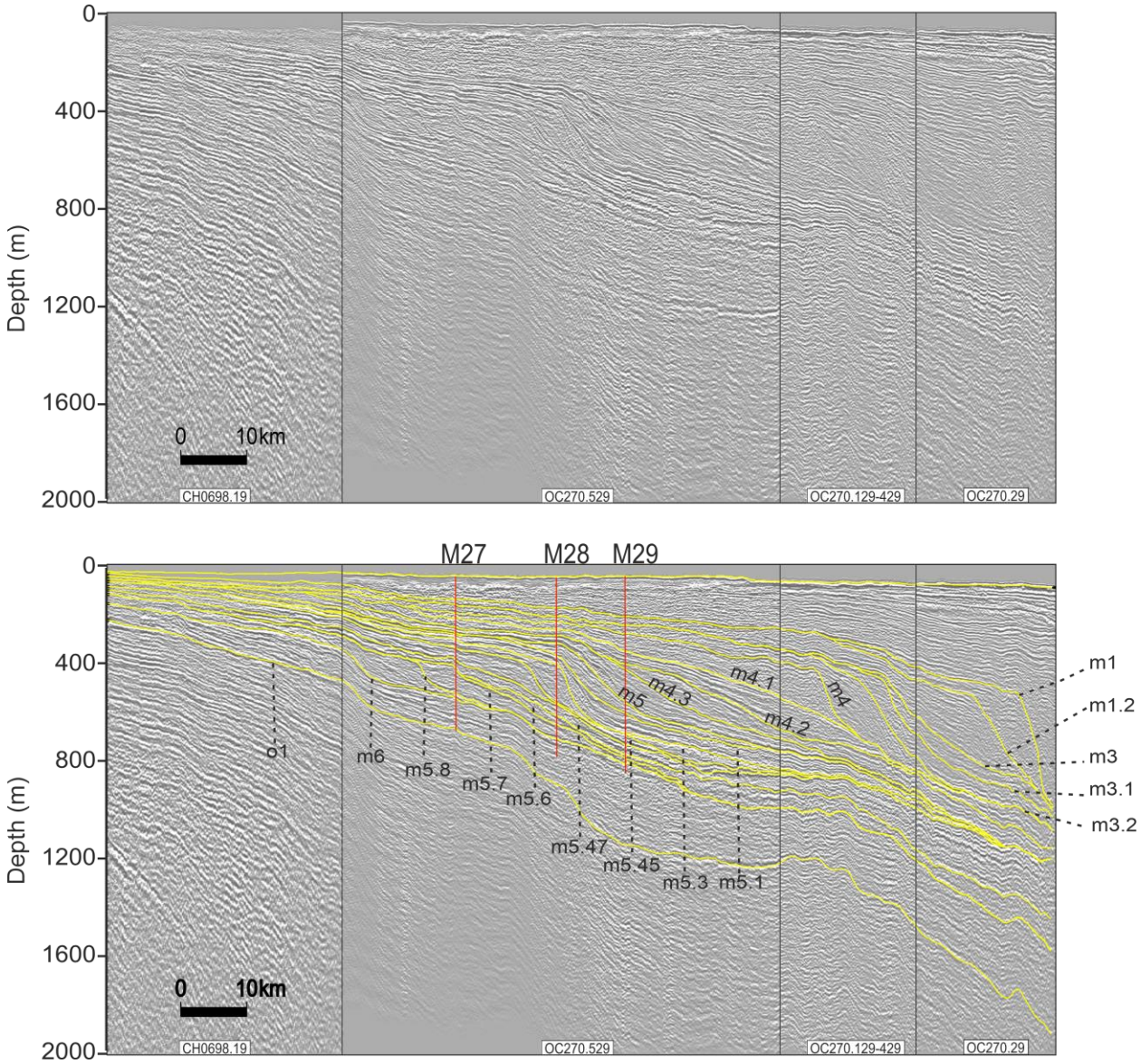

Figure 2 Seismic interpretation of New Jersey shelf sequences on adjacent 2D depth migrated lines CH0698.19, OC270.529, OC270.129-429, OC270.29

The stratigraphic framework, shown in Figure 2 was characterized with a facies distribution using Sequential Indicator Simulations (SIS). This stochastic approach is a variogram-based simulation of categorical variables, which can be constrained by well data as well as quantified geological trends (Deutsch and Pyrcz 2014). In our implementation of the SIS algorithm, stochastic realizations are constrained by estimated vertical and horizontal correlation lengths, seismic reflector orientation, as well as vertical and horizontal probability trends derived from interpreted well log data.

Well data of IODP expedition 313 (Mountain et al. 2010), and AMCOR well 6011 (Hathaway et al. 1979) were used to categorize the sediments into three facies types based on density logs. Mountain et al. (2010) reported that density measurements corresponded to lithological changes observed on core data. Therefore, we defined the following categories: sand ($\rho > 2\,050$ kg m^{-3}), silt (1820 kg m$^{-3} \leq \rho \leq 2\,050$ kg m^{-3}) and shale ($\rho < 1\,820$ kg m^{-3}). The categorized well logs are shown in Figure 3. It must be noted that well 6011 is a projected well, which is approximately 10 km offset from the model transect. Despite this lateral offset, we assume the lithological information derived from the well can be considered representative for the sediment column in the proximal part of the shelf. Including this well data in the stochastic modelling process introduces an additional control point and reduces the uncertainty in the proximal part of the shelf.

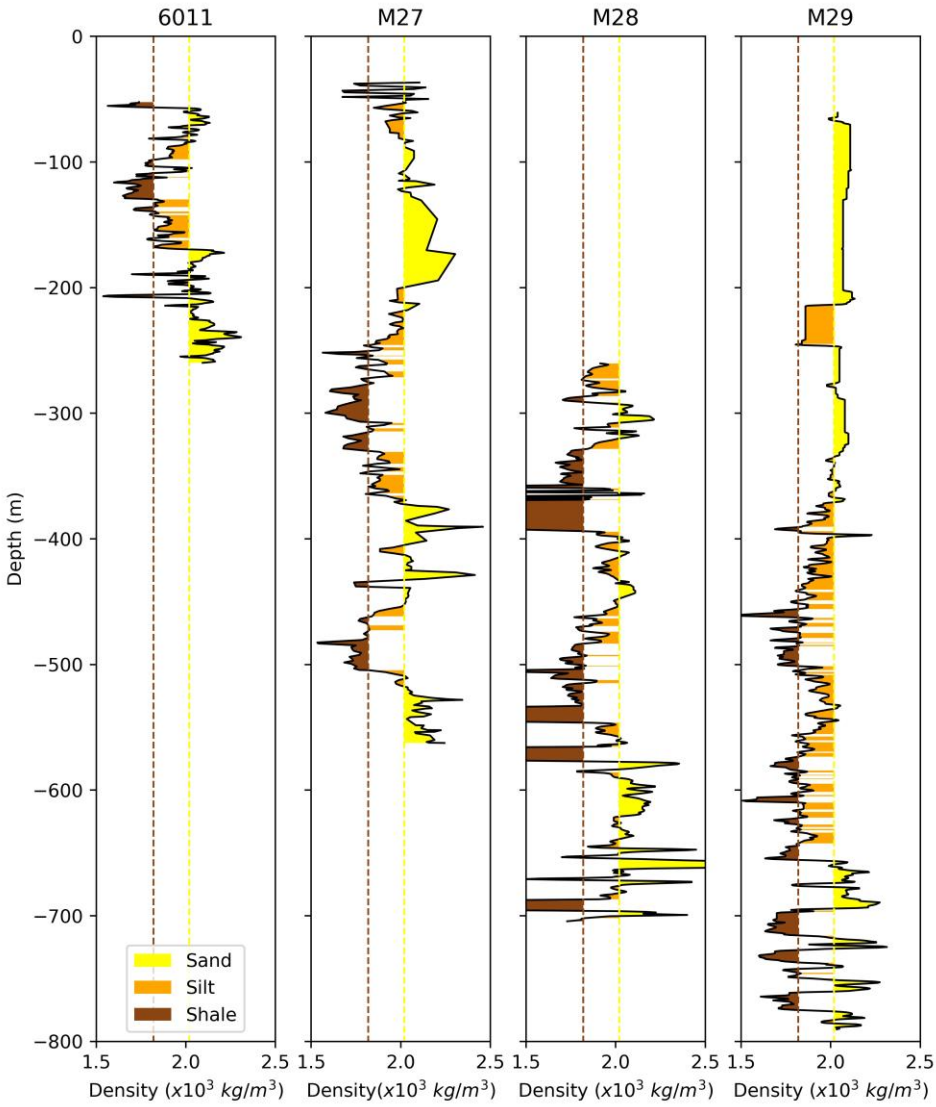

Figure 3 Interpretation and categorization of lithologies from bulk density data at well sites 6011, M27, M28, and M29. Mountain et al. (2010) reported that density variations in IODP Expedition 313 wells broadly correspond to lithology.

The categorized well log data were used to derive 1D facies probability functions. The horizontal facies probability function was defined by linear interpolation of control points, each corresponding to a single well. We calculated the probability of occurrence of each category over the entire well. This probability was defined for each facies category as $P_i = n_i/n_T$, where n is the number of samples of the category denoted with subscript i, and n_T is the total number of samples. In the absence of well data, a distal control point was assigned at the boundary of the model domain. At this location, we assume $P_{shale} = 0.75$, $P_{sand} = 0.1$ and $P_{silt} = 0.15$. This method of using

231 the proportion of each facies is a standard approach to incorporate geological trends into stochastic
232 models (Deutsch and Pyrcz 2014). In deltaic environments like the New Jersey shelf, it is typical
233 that fine-grained sediments are transported further basinward, resulting in a general offshore fining
234 trend in the lithology (i.e., increasing probability of shale). The trends obtained from four wells is
235 shown in Figure 4.

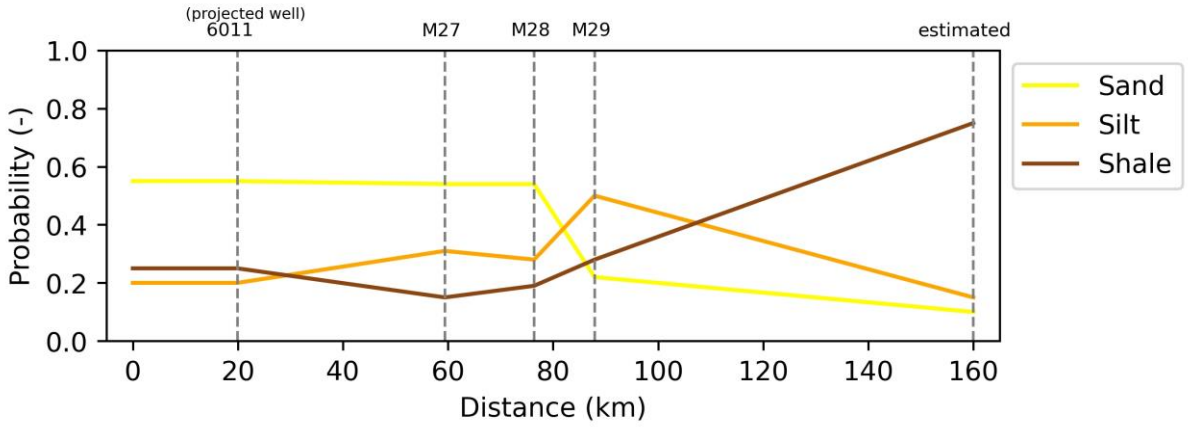

236
237 *Figure 4 Horizontal facies probability functions calculated by linear interpolation between control points.*

238 The horizontal trends were assigned globally for the model domain. Vertical trends were
239 incorporated by calculating vertical proportionality curves for each sequence individually using
240 well data analysis tools in Petrel. These trends jointly contrain the sequential indicator simulation
241 algorithm and incorporate realistic geological features into the suite of models produced. The
242 model domain is thereby populated with the three facies types, to which petrophysical properties
243 were later assigned for numerical simulation. Cemented intervals identified by core analysis
244 presented in Lofi et al. (2013) were included deterministically in the model framework. These
245 high-density intervals lead to high acoustic impedance at the cemented regions of the sequence
246 boundaries (Miller et al. 2013a). We approximate the lateral extent of these cemented layers based
247 on the interpretation presented in Lofi et al. (2013) as well as the amplitude of the reflectors.

248 The final input to the stochastic model are the variogram parameters. In the absence of sufficient
249 well data for variogram modelling, we estimate the variogram parameters based on the
250 depositional model. The New Jersey clinothem system is penetrated at the topset, rollover and
251 bottomset positions by IODP wells M27, M28 and M29 respectively (Mountain 2010). This system
252 of prograding clinoforms is at least 22 km across and interpretation of sequences across the wells

has been established based on seismic data (Miller et al. 2013b), as well as biostratigraphic interpretation (Browning et al. 2013). Generally speaking, the dimensions of shoreface-shelf deposits for wave-dominated delta system have a wide range from a few kilometres up to 30 km (Hampson 2010; Reynolds 1999). The continuity of facies along the dip direction is determined by the shoreline progradation distance of the delta during the time of deposition. Using this model, we assigned a correlation length of 15 km for the variogram model as an average repsresentative value for the entire system. In addition to the correlation length, we defined a dip angle of maximum correlation for each sequence. This was determined from the average dip of the seismic reflectors in the sequence. These values ranged between 0.25° and 1.2°.

The matrix properties were assigned to the model domain based on the interpreted lithology. Porosity compaction trends were derived from core-sampled porosity data measured by Mountain et al. (2010). The data of each facies group was fitted to an empirical exponential equation first described by Athy (1930):

$$\theta = \theta_0 e^{-az} \quad (1)$$

where θ is the porosity at depth z (m), θ_0 is the initial porosity and a is the correlation coefficient. Two trends were derived based from the log data, a sand compaction trend and a silt/shale compaction trend. The three categories sand, silt and shale correspond to high, medium and low permeability, respectively. Matrix parameters are summarized in Table 1.

Table 1 Summary of matrix properties used in all simulations

Parameter	Value	Unit	Reference
Permeability	†9.4×10^{-12} *7.4×10^{-14} ††9.0×10^{-16}	m^2	(Lofi et al. 2013; Thomas et al. 2019)
Porosity	†$44.7\ e^{-2.46\times10^{-4}\ z}$ $57.5\ e^{-5.93\times10^{-4}z}$	-	(Mountain et al. 2010; Thomas et al. 2019)
Thermal conductivity	†2.9 *2.3 ††1.7	W m^{-1} K^{-1}	(Mountain et al. 2010)
Volumetric Heat capacity	†2.4×10^6 1.9×10^6	J K^{-1} m^{-3}	

† - sand, * - silt, †† - shale

2.2 Stochastic simulation and model selection

The SIS algorithm generates multiple stochastic realizations of equally probable scenarios, which honour the input data. However, SIS does not consider the connectivity of the model domain. The lateral flow connectivity is an important consideration in assessing the hydrogeologic evolution of the freshened groundwater reservoirs on the New Jersey shelf, and the potential role of modern day recharge. Connectivity of stochastic models are often assessed by calibration of facies distribution with field pumping data (Zhou et al. 2014). In the absence of such data for our study domain, we conducted a simple Monte Carlo sampling from a suite of 100 model realizations to select models to use for numerical simulations (Deutsch and Pyrcz 2014).

The steady-state solution of the hydraulic head was used to derive a simple metric that is related to an important aspect of the system, the onshore – offshore connectivity of the realization. This process-based model selection approach is a standard practice in geostatistical reservoir modelling (Deutsch and Pyrcz 2014). The models were initiated with hydrostatic conditions, and fixed head boundary conditions at the lateral boundaries such that a 25 m hydraulic head difference was maintained between the landward and oceanward boundaries. That value was chosen based on results presented in Cohen et al. (2010), which estimated that conditions during the LGM resulted in head values along the New Jersey that may have been 25 m higher than present-day. After calculating the steady-state solution, the horizontal distance between the land boundary and the average position of the contour representing a 10 m increase in head within the model domain was measured. A longer distance would correspond lower hydraulic gradient, an indication of higher flow connectivity between two points (Freeze and Cherry 1979). Based on the probability distribution of this distance, two model realizations were chosen for numerical simulations representing high- and low onshore-offshore connectivity scenarios. Numerical simulations were performed on both model scenarios.

Summary statistics calculated on the lateral distance to the 10 m contour line show an average distance of 48.4 km with a standard deviation of 27 km. The probability density function (PDF) was estimated using a gaussian kernel density estimation (Hastie et al. 2009). This is a non-parametric method that estimates the PDF of a continuous random variable. The PDF shown in

Figure 5, has a bimodal distribution, which points to low-to-intermediate connectivity as the more likely scenario given the currently available data. A less likely scenario is high connectivity.

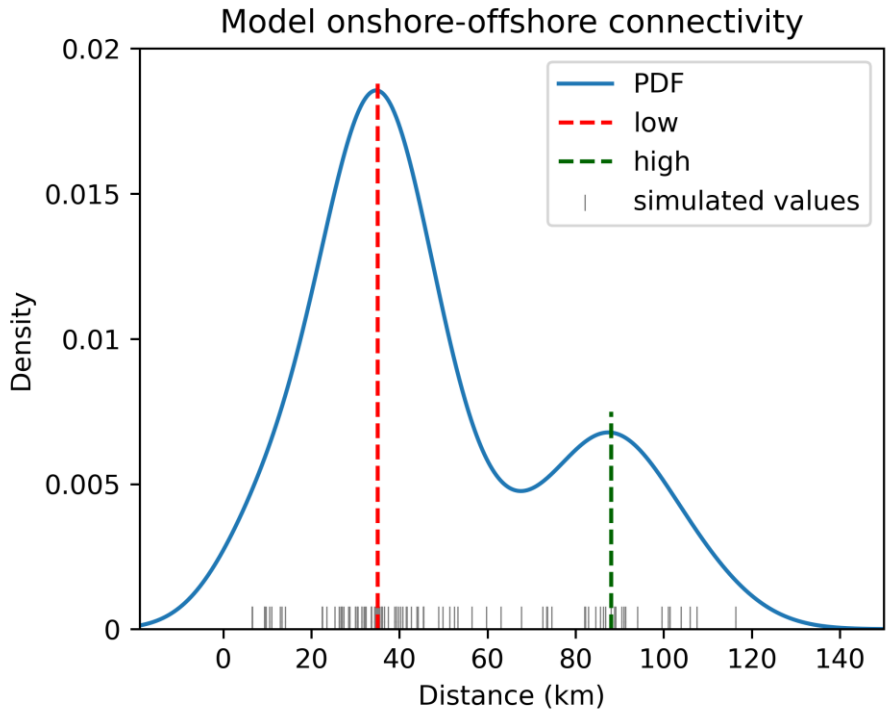

Figure 5 Probability density function of model connectivity metric showing a bimodal distribution for a suite of 100 stochastic model realizations. The positions of the low and high onshore-offshore connectivity modes are indicated by red and green dashed lines, respectively. The realizations with values closest to these two modes were selected for numerical simulation.

Based on these summary statistics, we conducted numerical studies using two realizations, representing low and high connected mode scenarios. The models with the connectivity values closest to the two modes were selected. The high and low connectivity scenarios were represented by realizations 97 and 51, respectively. These realizations are shown side by side in Figure 6. The steady-state hydraulic head contours are overlayed on the model domain.

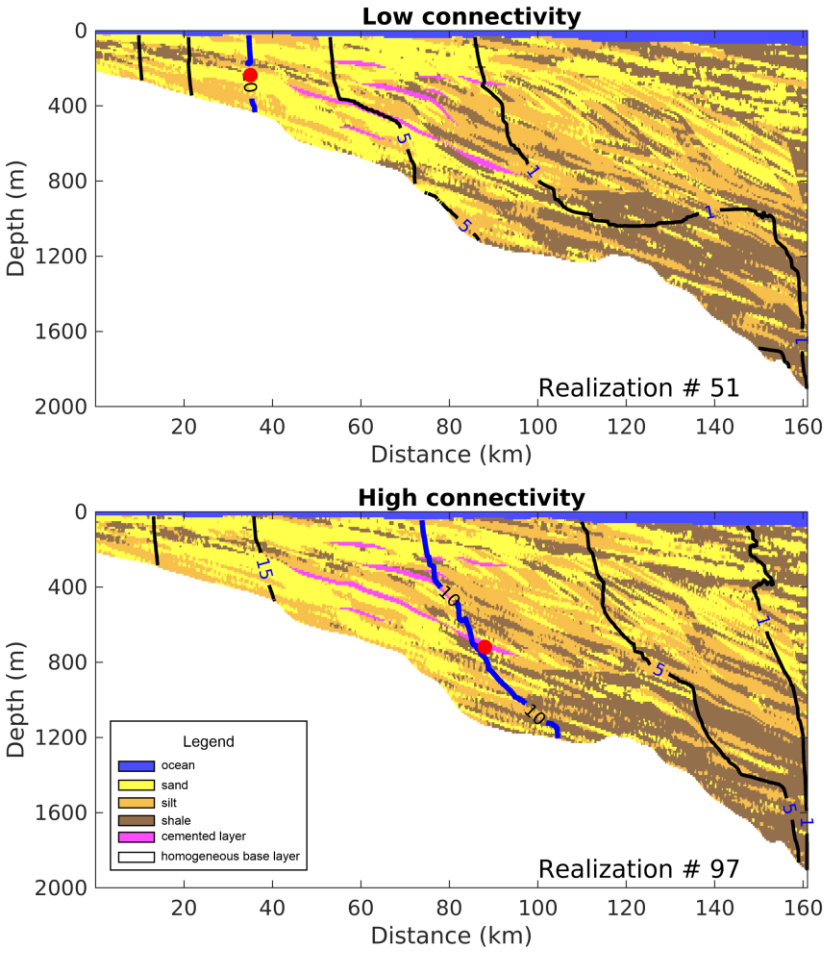

Figure 6 (a) Low onshore-offshore connectivity model (b) High onshore-offshore connectivity model realizations. Both models show the position of the 10 m hydraulic head contour in bold blue. The models were ranked based on the horizontal distance between the landward boundary and the average position of the contour indicated by the red dot. The corresponding porosity compaction models are included in the Supporting Information of this manuscript (Fig. S1)

2.3 Modelling the offshore freshened groundwater system

Numerical simulations were performed using a finite difference numerical modelling algorithm called SHEMAT-Suite (Clauser 2003; Keller et al. 2020; Rath et al. 2006). We simulate variable-density groundwater flow coupled with heat transport, taking into consideration the key drivers of fresh/saline groundwater flow on this regional scale model. Clauser (2003) provides a detailed description of the partial differential equations implemented in SHEMAT-Suite for groundwater flow, heat and solute transport. The parameters assigned to the flow model are the same as in Thomas et al. (2019). These are summarized in Table 2.

Table 2 Summary of model parameters used in all simulations

Parameter		Value	Unit	Reference
Fluid properties	Reference Density (freshwater)	1 000	kg m^{-3}	(Freeze and Cherry 1979)
	Compressibility	4.58×10^{-10}	Pa^{-1}	
	Viscosity	1.0×10^{-3}	Pa s	
	Thermal Conductivity	0.6	W m^{-1} K^{-1}	(Ramires et al. 1995)
	Specific heat capacity	4128	J K^{-1} kg^{-1}	(Siegel et al. 2014)
Solute transport	Molecular Diffusion Coefficient	1.1×10^{-9}	m^2 s^{-1}	(Freeze and Cherry 1979)
	Molar Mass (NaCl)	58.44	g mol^{-1}	(Manahan 2011)
	Dispersivity	50	m	(Gelhar et al. 1992)

We simulated 70 000 years of the Pleistocene lowstand. During this period, the sealevel fell as low as 120 m relative to present-day (Imbrie et al. 1984). As a result, large areas of land were subaerially exposed on the low-angle passive margin platform of the New Jersey shelf. For the purpose of this analysis, we define two distinct phases of this period. The recharge phase from 70 000 to 12 000 years BP, and the flooding phase from 12 000 years BP to present day. That starting point was chosen as it is approximately when the entire transect of the ocean floor (Figure 2) became subaerially exposed. A set of idealized simulations were designed to investigate the sensitivity of freshwater emplacement as hydraulic conditions on the shelf responded to sea-level lowstand.

The numerical study is presented in two phases. Firstly, we assess the model sensitivity to topographic-driven flow (base case), cemented intervals, enhanced terrestrial discharge and permeability anisoptropy. Topographic-driven flow refers to the lateral hydraulic gradient induced by the seafloor topography. We consider this the base case, as the shelf exposure is the essential condition that allows meteoric recharge. The cemented intervals have been identified in core samples, and found to be correlated with the fresh – saline pore fluid boundaries reported in previous petrophysical studies (Lofi et al. 2013; Mountain et al. 2010). We simulated a hypothetical scenario in which these intervals were assigned regular matrix properties of silt (Table 1), in order to quantify their impact. Enhanced terrestrial discharge (ETD) refers to offshore-directed flow generated at the landward boundary of the model, accounting for a subterranean influx of freshwater. This was modelled by an increased hydraulic head at that boundary. The

assigned value was based on computed heads during the Pleistocene and Holocene along the Atlantic continental shelf modelled by Cohen et al. (2010). Their simulations accounted for conditions induced by ice sheet loading and sealevel fall, and estimated up to 25 m increase in hydraulic head on-shore in the region near our model transect. Finally, we investigate the influence of anisotropic permeability. Anisotropy is a common feature in sedimentary environments due to the influence of bedding and possible compaction banding (Holcomb and Olsson 2003; Vajdova et al. 2004). In this study, we define the anisotropy in terms of the ratio of horizontal permeability, k_h and vertical permeability, k_z. We consider two plausible values of the anisotropic ratio, two and ten. The set of simulations described above was conducted on both high and low connectivity model realizations. Boundary conditions for all scenarios are summarized in the following section. The scenarios were compared based on three observation criteria. Firstly, the volumetric trend of fresh pore fluid in the model domain over the simulated time. Although the model is 2D, the volumes were calculated based on the cell with of 100 m, and the pore volume of each cell. Secondly, the present-day pore fluid concentration profiles were compared to measured data at the four wells sites for each scenario. Finally, the pore fluid concentration distribution in the model domain was analysed at two key times, the end of the recharge phase and at present day to consider the role of geological heterogeneity.

In the second phase, we conduct a comprehensive set of simulations on a single representative model realization, designed to reconstruct conditions over the period from 70 000 years BP to present-day. For this phase, we consider only the low onshore-offshore connectivity realization (Fig 6 a), as it corresponds to the highest likelihood based on the probability distribution (Fig. 5). We consider the compounded effect of topographic-driven flow, enhanced terrestrial discharge and permeability anisotropy. At the end of these simulations, the pore fluid concentration in the model domain was compared to present-day observations in IODP Expedition 313 wells and AMCOR well site 6011. This comparison, together with the distribution of freshened groundwater in the model domain is analysed to draw conclusions about the dynamic nature of the OFG system.

The volume of freshwater in the model domain over time is considered as a metric for quantifying the influence of the abovementioned factors. Ocean water has a total dissolved solid (TDS) concentration of approximately 35 g L^{-1}. For the purpose of this study, the modelled solute is NaCl, which has a molar mass 58.443 g mol^{-1}. This translates to, and is specified in SHEMAT-Suite as

a molecular concentration of 0.6 mol L^{-1}. In this study, pore fluid is defined as freshwater when it has a solute concentration of less than 0.3 mol L^{-1}, i.e., approximately half the TDS concentration of seawater (~17.5 g/L TDS).

2.3.1 Initial and boundary conditions

The coupled variable-density flow and heat transport simulations in this study require compatible boundary conditions for groundwater flow, heat and solute transport. The boundary conditions were designed to be consistent with laws of conservation of mass and energy within the model domain. All simulations were initialized under the same conditions to facilitate comparison.

The initial temperature and hydraulic head distribution in the model domain were set to the steady-state solution of their respective equations. For temperature, surface cells were assigned a Dirichlet boundary condition of 4 °C, representing the average surface temperature during the recharge phase (Johnsen et al. 1995). Basal specific heat flow was prescribed by a Neumann boundary condition of 0.06 W m^{-2} (Lachenbruch and Sass 1977). The groundwater flow was constrained by a Dirichlet boundary condition assigned along the surface cells and lateral boundaries. The head in each surface cell was set to its elevation relative to the model datum. At the landward and oceanward boundaries, the head was set to the elevation of their respective surficial cells. We invoke the simplifying assumption that the hydraulic gradient mirrors the surface topography, and consider only saturated flow (Freeze and Cherry 1979). Determining initial salinity distribution is challenging as the position of the freshwater – seawater interface is transient and dynamic (Meisler et al. 1984). We assume the domain is fully saturated with saline pore fluid (0.6 mol L^{-1} or 35 g L^{-1} TDS) in all cells below sealevel, shown in Figure 7. This represents a conservative initial estimate as it is likely that more freshwater recharge would have taken place as the transect was partially exposed i.e., prior to our simulated period. Therefore, the model may underestimate the volume of freshwater that would have been emplaced over the entire regressive – transgressive cycle. This initial condition has also been implemented in a comparable regional numerical study (Siegel et al. 2014). The assumption isolates the simulated period as a minimum baseline for recharge, and provides a reference point from which to ascertain whether older freshwater emplacement is needed to explain the present-day observations.

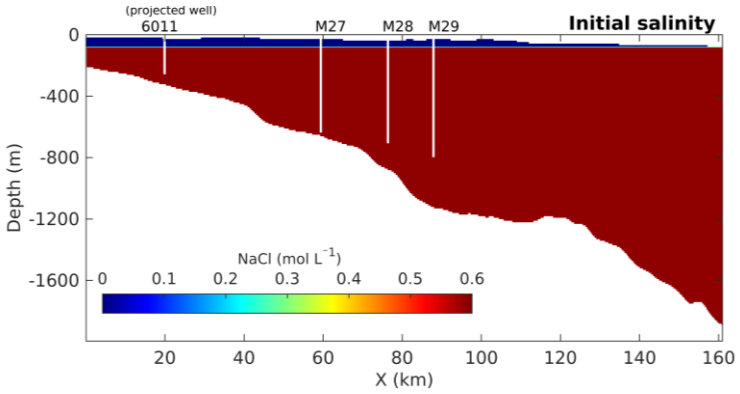

Figure 7 Initial salinity distribution in model domain. All cells below initial sealevel initialized at 0.6 mol L^{-1} / 35 g L^{-1} TDS

During the recharge phase, surface temperature was fixed to the initial condition described above, with the steady-state thermal gradient at the lateral boundaries. Dirichlet boundary condition of zero salinity was assigned to the model surface. This represents meteoric recharge, which is known to have negligible salinity (Selley and Sonnenberg 2015). The landward and oceanward lateral boundaries were set to 0.0 mol L^{-1} and 0.6 mol L^{-1}, respectively. The hydraulic head at the surface and landward boundaries were set to the surface elevation. The unsaturated zone and associated infiltration processes are assumed to be negligible. This assumption is validated considering the large aspect ratio between the model length and the depth of the sediments under investigation (Freeze and Cherry 1979).

At the oceanward boundary, we assigned a time-varying Robin boundary condition. This specifies flow across the model boundary using the formulation as described in Jazayeri and Werner (2019):

$$Q = -\frac{\mathrm{KA}}{\mathrm{L}}\,(\mathrm{h} - h_{\mathrm{ref}}) \qquad (2)$$

where K (m s^{-1}) is the hydraulic conductivity of the extended region, A is the cross-sectional area of the boundary, $\mathrm{h} - h_{\mathrm{ref}}$ (m) is the head drop between the model boundary and an external reference point and L (m) is the distance between the model boundary and that point. The reference head, h_{ref} is the sealevel elevation at the shelf edge. The values were sampled from the relative sealevel curve by Imbrie et al. (1984) at 2000 year intervals, as summarized in Figure 8. This type of boundary condition is applied as our model transect does not extend all the way to the shelf edge. This head dependent flux approximates the hydraulic conditions of the shelf region outside of the model domain.

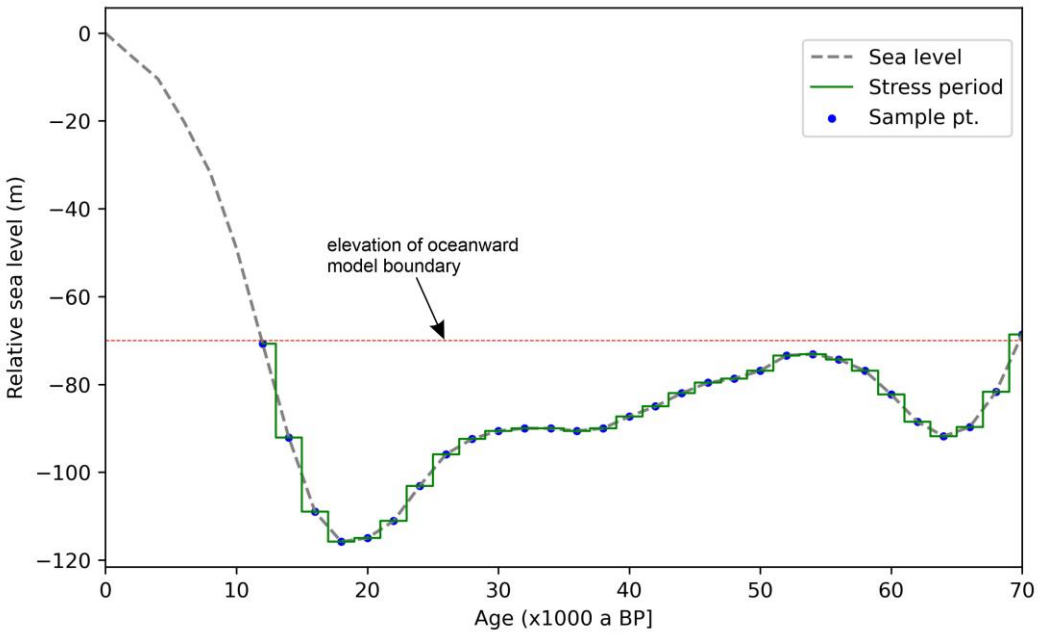

Figure 8 Relative sea level curve of the past 70 000 years used to determine boundary conditions for model domain. Blue dots show the sample points (h_{ref}) and light green lines indicate 2000 year period for which the value was applied. The red dashed line represents the level of the model's oceanward boundary (h).

For our model domain, A = 1.92×10^5 m^2 based on the cell dimensions, and the distance from the model boundary to the shelf edge L = 25 000 m. We estimated a value of K = 7.6×10^{-8} m s^{-1} as the average hydraulic conductivity for the distal section of the shelf. The main model boundary conditions during the recharge phase are summarized in Figure 9. The conditions were applied in all cases with the exception of ETD. In that scenario, shore-parallel flow was enhanced by increasing the head at the landward boundary by 25 m.

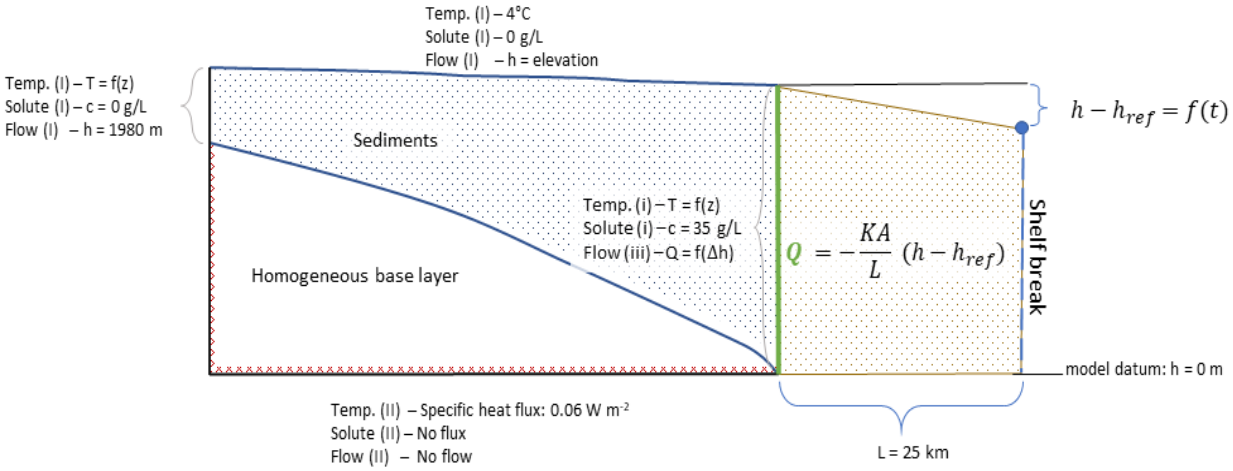

Figure 9 Recharge boundary condtions. (i) Dirichlet type boundary condtions, (ii) indicates Neumann type boundary conditions, and (iii) Robin boundary condition. Red hashed line represents no flow conditions assigned to the homogeneous base layer.

449 Flooding Phase

450 During the 12 000-year period of Holocen transgression, the topographic flow regime of the
451 recharge phase passes over into today's hydrostatic conditions. Each model run was initialized
452 using pore fluid concentration obtained at the end of the corresponding recharge phase. Time-
453 dependent boundary condition functions were implemented in SHEMAT-Suite to represent a
454 transgressing coastline during the simulated period. The hydraulic head at surface cells was
455 increased to sea-level elevation as the model domain is gradually flooded. The head at the
456 oceanward boundary was intiated at the surface elevation and increased over the transgressive
457 period to the present-day sea level at that point of the shelf. The head at the landward boundary
458 was set to 5 m above surface elevation. The salinity of the relevant surface nodes was increased to
459 ocean salinity according to the timing of the marine transgression. The surface temperature was
460 also increased linearly from 4 °C to the present-day average sea-surface temperature of 14 °C
461 (O.S.P.O. 2013). Temperature at the lateral boundaries was fixed to the steady-state thermal
462 gradient.
463

3 Results

3.1 Numerical simulation of freshwater emplacement

In the following sections the results of the numerical simulation are presented in detail. Firstly, we present observations of the freshwater emplacement mechanism in the context of a heterogeneous shelf model. This is followed by sensitivity analysis comparing the influence of various hydrogeologic scenarios. Finally, we present a paleo-hydrogeological reconstruction of the LGM on a representative shelf model.

3.1.1 Analysing the mechanism of freshwater emplacement

This section presents the results of topographically driven flow for both high and low onshore-offshore connectivity cases, abbreviated as HC and LC, respectively. The mechanisms by which freshwater is emplaced in the sediments are analysed in the context of the heterogeneous shelf models.

Figure 10 shows the progressive freshening of the shelf sediments in the base case in the low onshore-offshore connectivity model. The figure shows snapshots of the recharge phase taken in the periods between 68 ka BP to 64 ka BP, and 28 ka BP to 12 ka BP. These correspond to the periods of most rapid sealevel change (see Fig. 8) and the most observable changes in pore fluid concentration. It can be observed that due to topographically driven flow during the simulated sea-level lowstand, freshwater is emplaced across the entire shelf transect to varying depths. The interface between fresh and saline water is highly complex as a result of the geological heterogeneity. The depth of freshening becomes gradually more shallow in the oceanward direction. The result indicates that the offshore directed hydraulic gradient resulting from surface topography is sufficient to drive freshwater into sediments across the entire shelf transect. The most distal part beyond 120 km from the shore is relatively flat, leading to much slower rates of freshening. In general, a downward movement of the fresh – saline interface occurs in response to a sea-level lowstand. Top-down freshening by surface derived recharge appears to be the primary mechanism driving the emplacement of freshwater. In a topographically driven flow regime, the recharge is focussed into high permeability intervals (Hobbs and Ord 2015). As a result of the hydraulic gradients, recharged freshwater is driven laterally into aquifer units, while overlying

confining units remain saline for a longer period. Furthermore, this preferential flushing of permeable intervals causes density instabilities, resulting in density-driven free convection between the saline pore fluid in the confining units and the underlying freshened aquifer units.

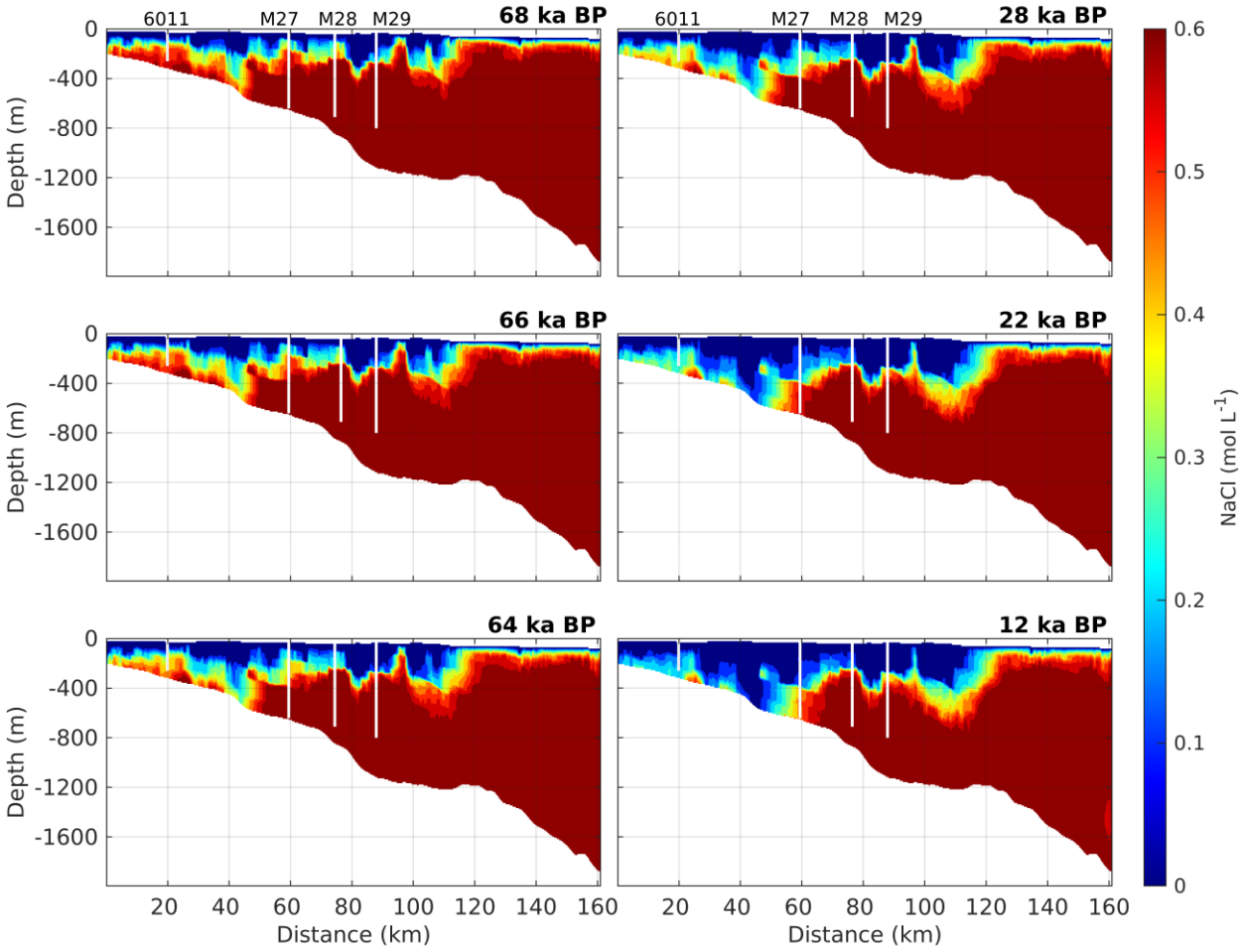

Figure 10 Solute concentration in the model domain during the recharge phase for the base case scenario in the low onshore-offshore connectivity model realization. Snapshots of the transient results show the complexity of freshwater recharge in the heterogeneous subsurface. Freshening occurs by a combination of advective flow in aquifer units and density-driven free convection in confining units. Freshening appears to occur primarily from the surface recharge.

The recharge phase displays similar dynamics in the high onshore-offshore connectivity model, shown in Figure 11. These results indicate that the recharge of freshwater during lowstand is primarily a function of topography and geological heterogeneity. Marginal changes in the pattern of freshening can be seen in the proximal part of the shelf as a result of the higher onshore-offshore connectivity. However, the general position and shape of the fresh – saline water interface closely match the LC model.

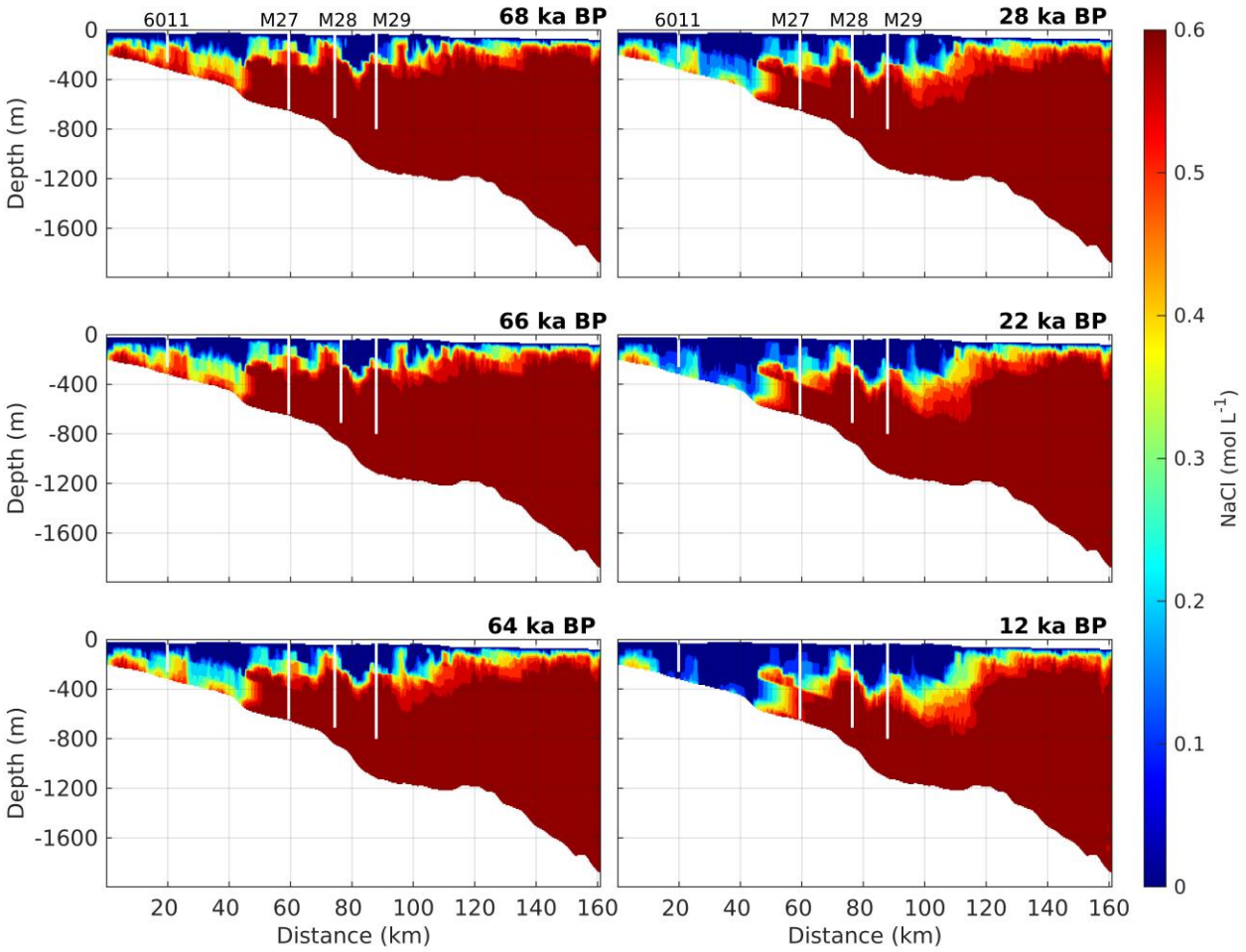

Figure 11 Solute concentration in the model domain during the recharge phase for the base case scenario in the high onshore-offshore connectivity model realization. The distribution at the end of the recharge phase (12 ka BP) shows more evidence of channelized flow of freshwater when compared to the low connectivity case. Top-down freshening by surface recharge is restricted by laterally continuous aquitards present in this model.

The pore fluid concentration at the end of the recharge phase is shown for both models in Figure 12. It can be observed that freshwater is driven deeper in proximal regions of the shelf, where the sediment column is primarily sandy. Toward the distal shelf regions, there is a decreasing trend in grain size, which correlates with shallower penetration of freshwater. The shape of the fresh – saline interface shows considerable lateral variability corresponding to the stratigraphic terminations of sandy units. This highlights the importance of capturing the sequence stratigraphic architecture. A local topographic high around 100 km also corresponds to relatively deeper penetration of freshwater recharge. As surface elevation increases inland, freshwater is driven deeper into the sediment column. Freshwater was driven as deep as 500 m in the region of IODP well M27, both high- and low-permeability intervals are completely flushed with freshwater. The region around M28 shows freshwater recharge occurring down to about 300 m depth. Deeper

freshening appears to be impeded by the presence of cemented and low-permeability intervals below 300 m.

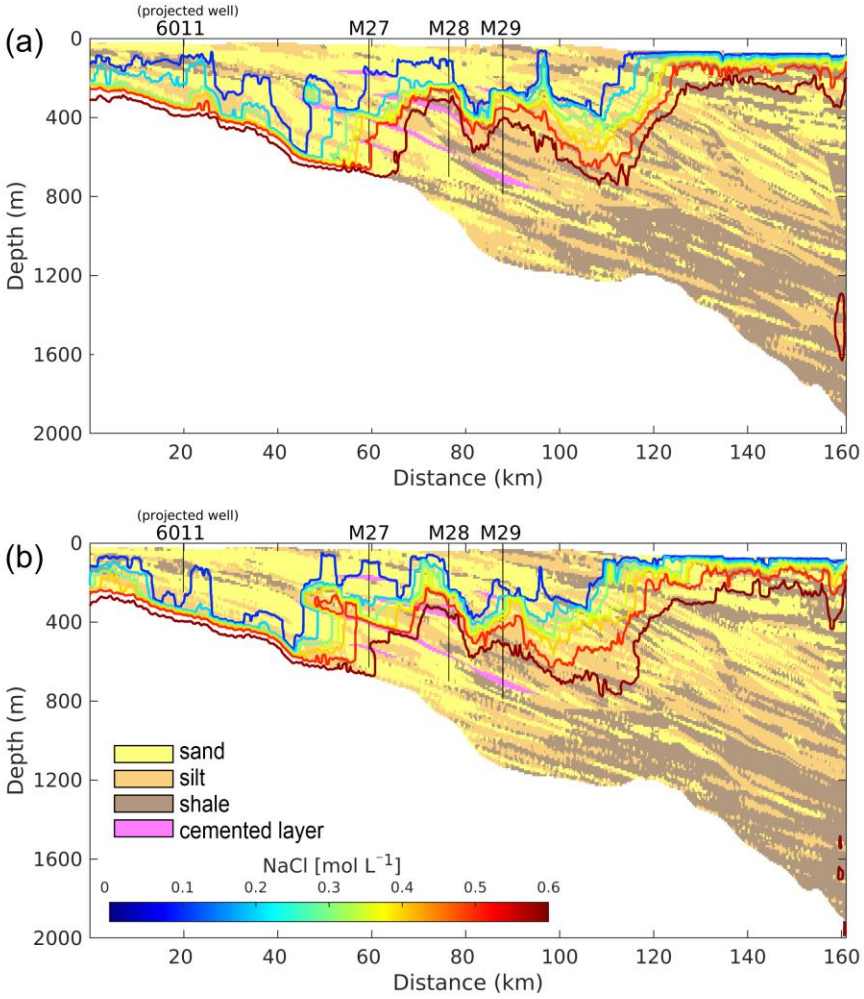

Figure 12 (a) Low onshore-offshore connectivity, (b) High onshore-offshore connectivity. Pore fluid concentration contours in model domain at the end of the recharge period (i.e. 12 000 years BP) overlaid on the facies model highlighting the correlation between geological heterogeneity and the distribution of freshwater recharge.

The presence of low-permeability sediments near the surface is a feature of the subsurface heterogeneity that strongly influences freshwater recharge. The HC model, shown in Figure 12 b, features some near-surface shale intervals in the mid-shelf region between 50 km – 80 km which are absent in the LC model. While these aquitards create conduits that increase the lateral flow connectivity in the model domain, they also have the effect of reducing the depth of penetration of surface derived recharge. This influences the extent to which the underlying sediments are freshened in the HC model relative to the LC model. The effect can also be observed in the proximal region of the models where more freshening occurs in the HC model due to

discontinuities in the confining layers. The near-surface distribution of low-permeability sediments influences the emplaced freshwater volumes such that the LC model facilitates more recharge relative to the HC model. The relative volumetric trends are presented in the following section.

3.1.2 Sensitivity analysis

Freshwater volumetric trends

In this section we present the simulation results for all scenarios in the high onshore-offshore connectivity (HC), and the low onshore-offshore connectivity (LC) models. We compared the two model realizations based on three sets of observation: (1) freshwater volume trends over the simulated period, (2) fluid concentration at the end of the recharge phase and present-day, and (3) fit between observed and measured pore fluid concentration at well locations.

Figure 13 shows the freshwater volume trend for the 70 000 year simulated period in both model realizations. There are two periods of rapid increase in freshwater emplacement that coincide with rapid sea-level fall. These occur from 70 000 years BP to 60 000 years BP and about 28 000 years BP to 18 000 years BP. The time of relatively slower regression between these two periods is characterized by a gradual linear increase in the freshwater volume. This pattern is replicated in both the HC and LC model realizations. A key observation is that all the curves show a similar trend to the base case. This suggests that the dominant mechanisms during the lowstand are meteoric recharge and topographically driven flow.

Removing the cemented intervals resulted in a moderate increase in emplaced freshwater relative to the base case (10 % - 14 %). The volume that survived until present day was only marginally smaller than the base case (blue curves in Fig. 13). This suggests that while cemented intervals strongly influence the geometry of surviving freshwater reservoirs, they are not significantly more influential than low-permeability shales on the overall reservoir volumes.

The ETD scenario resulted in a 2.1 % increase in the freshwater volume for the HC model and < 1 % in the LC model realization. This result is consistent with the difference in onshore-offshore connectivity between both models. In our model domain, the sediment column on the landward

boundary is 300 m thick, therefore this may underestimate the amount of discharge that enters into the offshore environment e.g., through deeper connected pathways.

The anisotropic permeability scenarios had the most significant influence on the emplaced freshwater volume. In the case of a horizontal to vertical ratio of two, the freshwater volume was reduced by 20 % in the LC model and 12.3 % in the HC model, relative to the base case. In both models the present-day freshwater volume is approximately equal to the base case. The anisotropy reduces the emplaced volume, but also acts to preserve more of the emplaced freshwater during subsequent regression. An increase of the anisotropy ratio to ten, led to a further decrease in the emplaced volumes and a significant flattening of the volumetric trend. We observed a very dampened response to the periods of rapid sea-level fall. In that case, the freshwater volume was reduced by 57.7 % in the LC model and 54.6 % in the HC model relative to the respective base cases. In the presence of strong anisotropy, effectively all of the recharged freshwater is salinified during the subsequent flooding phase, as shown by the magenta colored curves in Figure 13. These observations highlight the significance of downward infiltration of meteoric recharge through the sediment column from the model surface.

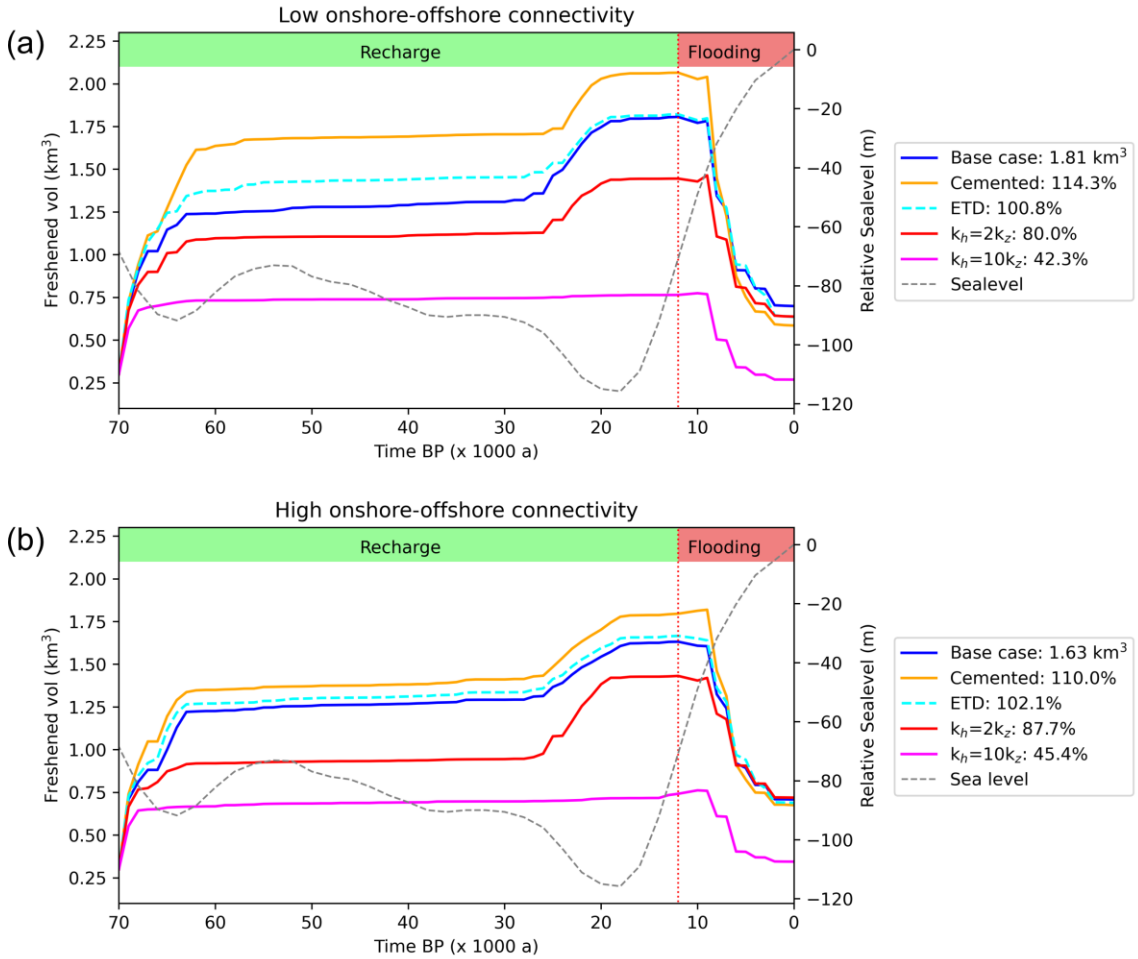

Figure 13 The volume of freshwater over the simulated period is plotted for all scenarios in (a) LC model and (b) HC model. The legend shows the volume of freshwater emplaced during the recharge phase for the base case, and the relative percentages at the end of the recharge phase are shown for all other scenarios. The dashed grey line shows the sea-level curve after Imbrie et al. (1984) plotted on the secondary y-axis (right).

Model concentration distribution

The distribution of pore fluid concentration in the model domain is shown at two key times i.e., the end of the recharge phase at 12 000 years BP, and present-day. We present results of the low onshore-offshore connectivity model in Figure 14, where each panel displays a different simulated scenario. In the recharge phase, we can observe that more freshening occurs in the region of M27 in the absence of cemented intervals (Figure 14 b). The ETD scenario shows only minor changes in the distribution within a range of 20 km from the landward boundary (Figure 14 c). Figure 14 (d) and (e) show the low and high anisotropy ratio cases, respectively. These result in an upward shift and general flattening of the fresh-to-saline interface. In the case of high anisotropy, freshening only occurs to ~ 300 m. With the exception of the high permeability scenario, the present day

distributions consistently reproduce a seaward-dipping zone of fresh water extending from the landward boundary to ~ 40 km offshore. Downward fingering of saline pore fluid can be observed separating the freshwater interval at site M27. In the case of low anisoptropy, this separation is characterized by a relatively brackish zone. The simulated results indicate another freshwater reservoir that extends oceanward of site M29. This reservoir has a sharp upper boundary that is seaward dipping in correlation with the sedimentary bedding. The salinity gradually increases with depth and distance offshore. This shallow body is preserved by near-surface low permeability intervals. The most distal regions of the shelf models show complete salinization of all emplaced freshwater. There is a broad region of fluid concentration that is just below ocean salinity.

The numerical simulations with the high onshore-offshore connectivity model display similar concentration distributions as described in the previous paragraph. The results are shown in Figure 15. In general, the proximal region of the shelf appears to undergo more freshening during the recharge phase in all scenarios. Thick sand intervals in the HC model facilitate more advective flushing with freshwater during the recharge phase. However, while the present day distributions are broadly similar to the LC model, downward fingering of saline pore fluid results in more compartmentalization of the seaward dipping fresh interval. Key differences are observed in the the ETD scenario, where the proximal region of the model domain (0 km – 40 km) is completely freshened during the recharge phase.

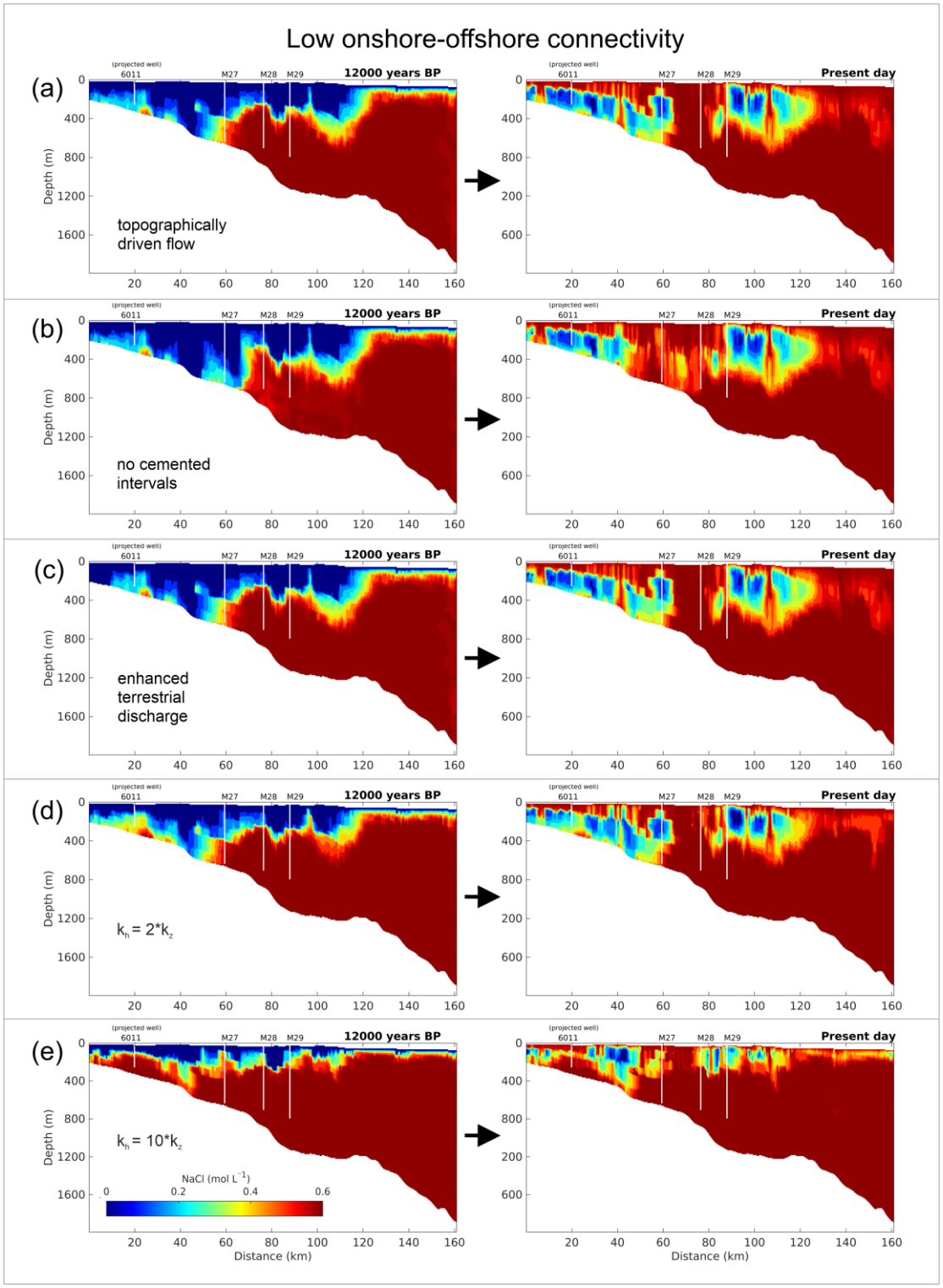

Figure 14 Low onshore-offshore connectivity model showing pore fluid concentration at the end of the recharge phase (left) and present day (right) for simulated scenarios: (a) Base case, (b) cemented intervals, (c) enhanced terrestrial discharge, (d) - (e) anisotropic permeability.

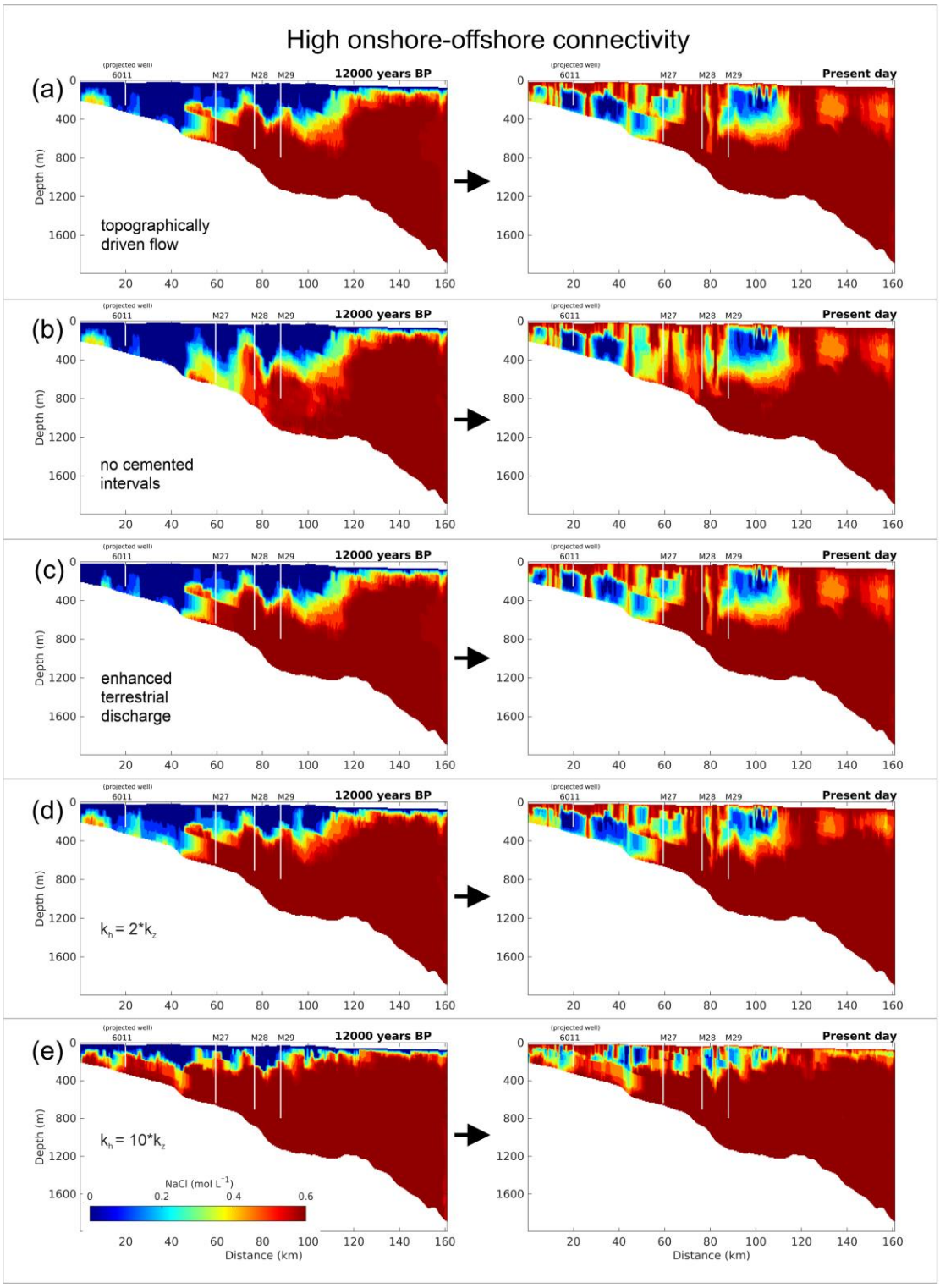

Figure 15 High onshore-offshore connectivity model showing pore fluid concentration at the end of the recharge phase (left) and present day (right) for simulated scenarios: (a) Base case, (b) cemented intervals, (c) enhanced terrestrial discharge, (d) - (e) anisotropic permeability.

628 Borehole pore fluid concentration profiles
629
630 Figure 16 shows the pore fluid concentration profiles extracted at the four well locations in both
631 model realizations. A close fit between simulated and measured data is observed at site 6011 in
632 both cases. All scenarios closely match the measured concentration with the exception of the high
633 anisoptropic ratio. In the HC model, the profiles show lower concentrations compared to the LC
634 model, consistent with increased offshore directed flow of freshwater from the landward boundary.
635
636 At M27 there are two major freshwater intervals, an upper reservoir between 200 m – 400 m with
637 sharp boundaries, and a shallow interval characterized by a sharp upper boundary and gradually
638 increasing pore fluid concentration with depth. The upper reservoir is replicated with slightly
639 higher solute concentrations in both model realizations. In the case of high anisotropy and the
640 absence of cemented intervals, both models do not capture this upper reservoir. In the case of high
641 anisotropy, this reservoir is not freshened during the LGM (see Figure 14). In the absence of
642 cemented intervals we observe a salinization of the entire sediment column in the region of M27.
643 The lower reservoir is not reproduced in any of the modelled scenarios.
644
645 At well site M28, there is a stronger differentiation between the HC and LC models. The HC model
646 shows a fresh – brackish interval in the shallow part of the well (< 300 mbsf) in all scenarios,
647 which is consistent with the trend of the measured data. The LC model consistently over-estimates
648 the salinity in this region of the model. Given the close fit between the HC and LC models at the
649 more proximal M27, this misfit at M28 can be attributed to the differences in surface-connected
650 pathways in the two models rather than onshore-offshore connectivity (see Figure 12). The fresh –
651 brackish interval in the deeper section of the well is not reproduced exactly at the well location.
652 However, in the region around M28, both models show some brackish pore fluid down to ~500 m
653 (see Fig. 14).
654
655 The concentration profiles at site M29 closely match across all scenarios. The simulated results
656 generally represent the trend of the observed data, with a broad fresh – brackish zone in the upper
657 section of the well. The alternating fresh – saline intervals have been attributed to thin shale beds
658 on the centimetre scale (Mountain et al. 2010), which are below our model resolution. In the deeper

659 section of the well we observed some hyper-salinization of the pore fluid with a brine developing
660 at ~700 mbsf.
661

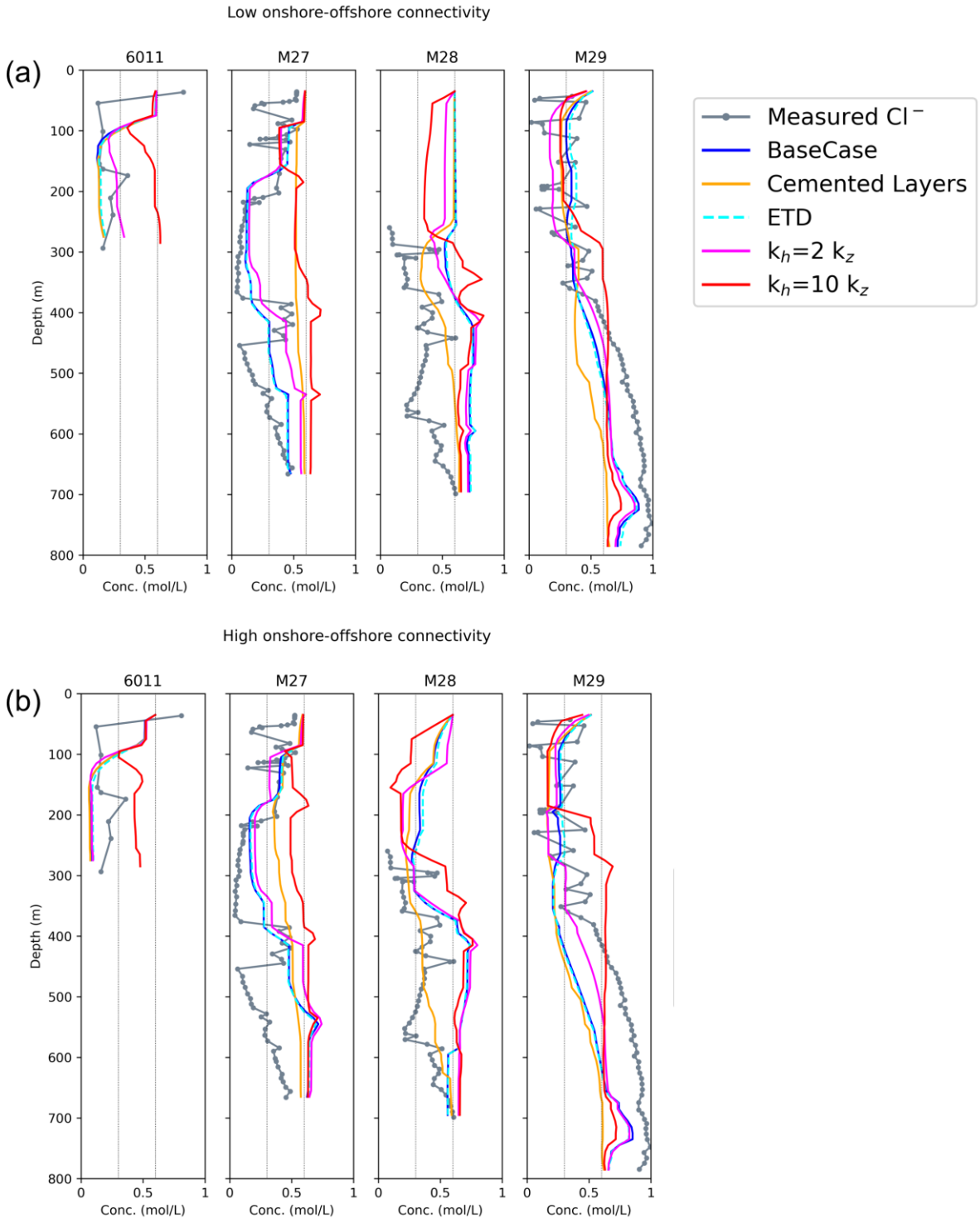

662
663 *Figure 16 Comparison between measured pore fluid concentration and simulated concentrations at 4 well locations in the model*
664 *domain. The low onshore-offshore connectivity model is shown in (a) and high onshore-offshore connectivity model.*

3.1.3 Paleo-hydrological reconstruction on a representative shelf model

This section presents the results of simulating conditions over the past 70 000 years until present day, with a plausible combination of scenarios on a single representative model. Based on the probability distribution of the suite of models (see Figure 5), we select the low onshore-offshore connectivity model as the representative case.

The transient simulation results are shown in Figure 17 for the isotropic permeability case. The simulated present-day distribution shows a laterally extensive system of offshore freshened groundwater with geometries correlating to the stratigraphic sequence boundaries on the shelf. Surviving freshwater intervals are generally oceanward dipping with sharp upper boundaries. Three main reservoirs can be identified in the present-day distribution (Figure 17 d). A thick interval of freshwater extending from the landward boundary to about 40 km offshore (labelled R1). In the region of site M27, a second freshwater reservoir is preserved by cemented and low-permeability layers (labelled R2). Downward fingering of saline pore fluid around 40 km in the model domain disconnects this reservoir from R1. Another laterally extensive zone of preserved freshwater extends about 30 km oceanward from site M29 and becomes gradually more saline – R3. This reservoir also appears to be compartmentalized by downward fingering saline pore fluid. The more distal region is characterized by a relatively well mixed zone of pore fluid just below seawater concentration.

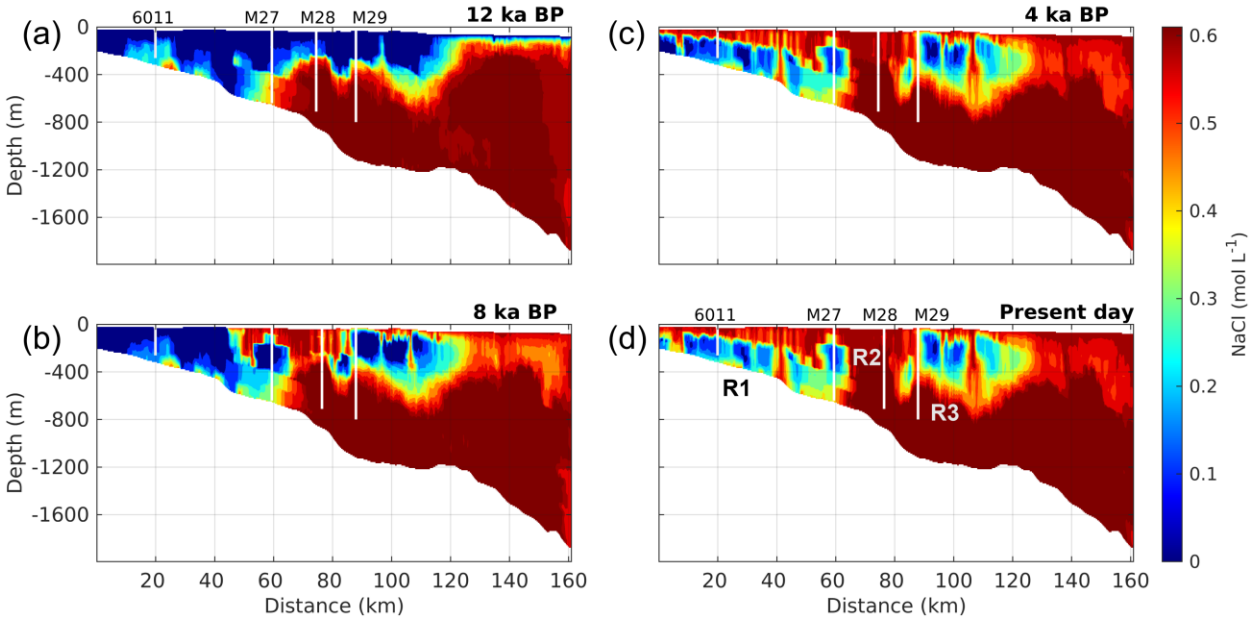

Figure 17 Simulated pore fluid concentration on a geologically heterogeneous 2D model of the New Jersey shelf. Progressive salinization of emplaced groundwater is shown from the onset of the marine transgression 12 000 years ago (top left) to the present-day (bottom right). The surviving freshwater reservoir system is laterally extensive but compartmentalized by downward fingering of saline pore fluid via discontinuities in confining layers.

The results show that downward fingering of saline pore fluid during transgression occurs via seafloor-connected pathways. The denser fluid begins to diffuse laterally when low-permeability or cemented layers are encountered. This can lead to the observed alternating fresh and saline pore fluid intervals. The transient results of the transgressive period for the anisotropic permeability scenario ($k_h=2k_z$) are shown in Figure 18. The general observations are consistent with the isotropic

case. However, R1 and R2 are now separated by a zone of brackish pore fluid. The preserved intervals are marginally thinner in the presence of anisotropy.

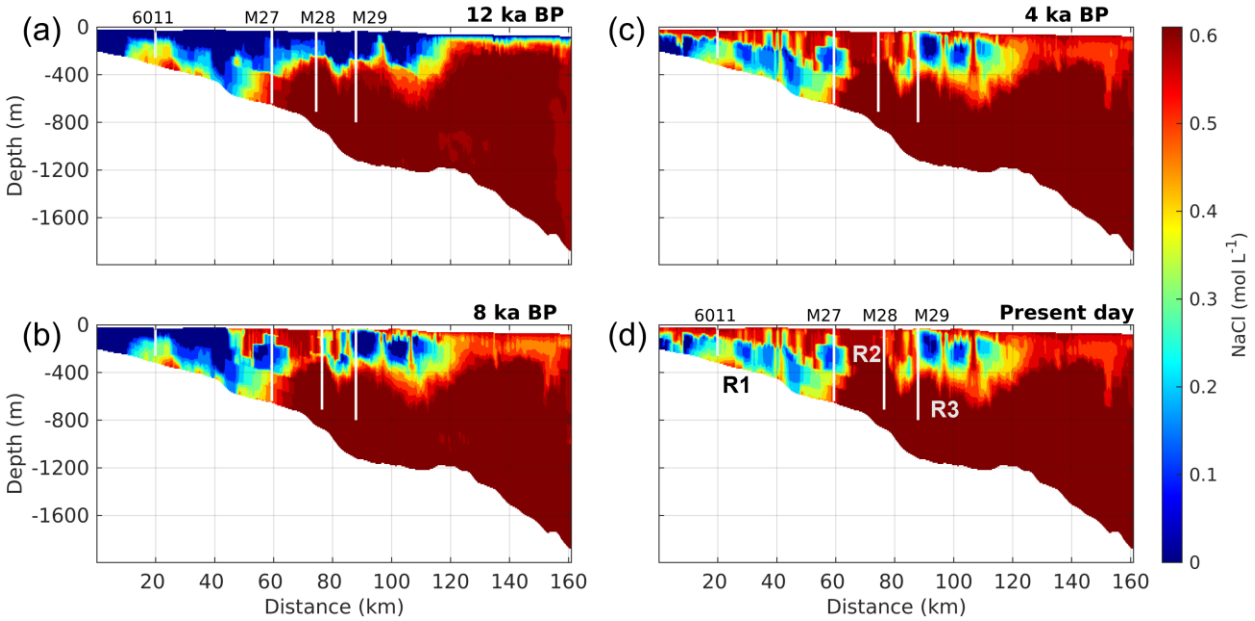

Figure 18 Simulated pore fluid concentration on a geologically heterogeneous 2D model of the New Jersey shelf with anisotropic permeability where $k_h=2k_z$. Progressive salinization of emplaced groundwater is shown from the onset of the marine transgression 12 000 years ago (top left) to the present (bottom right). The surviving freshwater reservoir system is laterally extensive but generally thinner than the isotropic permeability scenario.

The volumetric trend shown in Figure 19 a, shows that although more freshwater recharge is emplaced during the isotropic permeability scenario, the surviving fresh water volumes are effectively the same. The system shows a net increase in the volume of freshwater that is stored over the regressive – transgressive cycle.

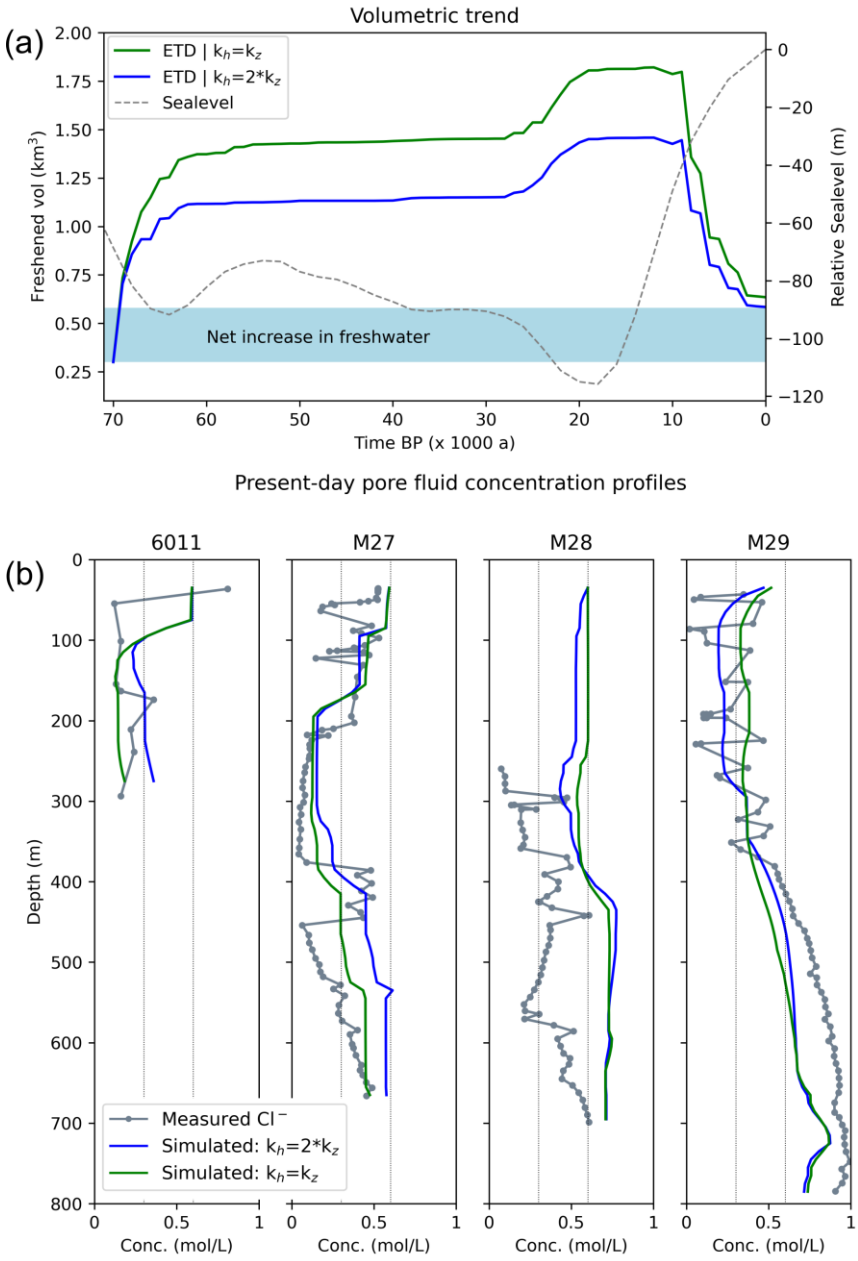

*Figure 19 Summary of key metrics for two simulated paleo-reconstructions: enhanced terrestrial discharge (ETD) with isotropic permeability (green), and ETD with k_h=2*k_z (blue) (a) Freshwater volumetric curve for the paleo-reconstruction of the LGM on the representative 2D New Jersey shelf model. The shaded blue region shows the difference between the initial assumed volume of freshwater in the model domain and the present-day volume, highlighting the net increase in freshwater storage. (b) Comparison of measured and simulated concentration profiles at the borehole locations in the model domain. Blue curve shows the low-anisotropic permeability scenario, and the green curve shows the isotropic scenario.*

Simulated concentration profiles were compared to measured values at the well locations shown in Figure 19 b. At site 6011, both simulated profiles closely match the measured data. The freshwater preserved just below the seafloor in the measured data is not captured by the model. At site M27 both scenarios reproduce the main freshwater interval (200 m – 400 m) with marginally higher

concentration. However, the deeper reservoir was not captured by the model. Once again, the preserved freshwater just below the seafloor is not reproduced. At site M28, the models underestimate the amount of freshwater stored in the sediment column. However, more freshwater is preserved a few kilometres oceanward of this site. At site M29, the trend of the shallow multi-layered freshwater system is broadly captured down to approximately 350 m. Below this depth, the modelled salinities systematically underestimate the measured values, which might be influenced by buried evaporites. However, some degree of hyper-salinization is observed.

4 Discussion

The simulation results provide detailed insight regarding the importance of geological heterogeneity for the emplacement and subsequent preservation of freshwater into the sediments of the New Jersey shelf. The numerical analysis provides strong evidence that the hydrogeologic conditions on the shelf during the LGM, together with the sequence stratigraphic architecture can lead to a complex layered OFG reservoir system. We employed a stochastic modelling approach using the sequential indicator simulation (SIS) to populate the model domain with sand, silt and shale facies. The variogram based approach is capable of sufficiently representing the sedimentary patterns of the passive margin depositional setting on the shelf. That is a key consideration when choosing a modelling approach (Seifert and Jensen 1999). An extended discussion on the suitability of SIS for a 2D model of the New Jersey shelf is presented in Thomas et al. (2019). Additionally, our approach incorporates geological information in the form of stratigraphic boundaries interpreted on seismic data, and trends derived from borehole data. This has been shown to reduce uncertainty in geostatistical models (Labourdette et al. 2008)

The Monte Carlo sampling of stochastic realizations allowed us to rank the models based on a key system characteristic, i.e., onshore-offshore connectivity. This allows for the selection of appropriate realizations from the probabilistic model. Analysis of dynamic response data is a common way to reduce uncertainty in stochastic facies models as it carries information about flow connectivity in the model domain (Hill and Tiedeman 2006). Each model realization honours the available data and thus represents equally likely scenarios. It must be noted that the probability distribution obtained is a function of the specific conditions assigned to the suite of models. The conditions applied in this study were designed specifically to quantify the distribution of onshore-offshore connectivity in the suite of models. This approach can be adapted in future studies to investigate other components of OFG systems such as confining layer continuity.

4.1 What drove freshwater emplacement on the New Jersey shelf?

Our numerical study shows that periods of rapid sea-level fall during the LGM accelerated the flushing of shelf sediments with freshwater via meteoric recharge. During the period of relatively slow regression, the observed freshening trend is considerably flattened. The correlation between rapid sea level fall and increased recharge was persistent across all simulated scenarios. All other

influences were superimposed on this trend. This observed dynamic supports the hypothesis that sealevel fall drives vigorous freshwater flow toward the open ocean (Meisler et al. 1984). Previous numerical studies of OFG systems have shown the infuence of sealevel lowstand on freshwater emplacement (Micallef et al. 2020; Person et al. 2003) . However, our results highlight the particular influence of rapid rate of sea level fall. In general, the depth of freshwater recharge increased inland with surface elevation. A 3D numerical study of the US mid-Atlantic shelf by Siegel et al. (2014) highlighted the strong control of seafloor topography on fresh groundwater emplacement. On average, observed salinities were lower in the relatively elevated eastern region of their model over the simulated period. The New Jersey shelf has a gentle gradient, however it is not consistently seaward sloping. Ocean floor bathymetry shows a slightly elevated region just beyond the mid-shelf, 100 km from the coastline. This local topographic high corresponds to a deeper circulation of freshwater during the low-stand period in all scenarios considered. This is consistent with observations in a regional study by Siegel et al. (2014), where seafloor topography was shown to be responsible for convection cells driving the re-distribution of fresh and saline water to a depth of several hundred meters. In a study characterizing global offshore fresh groundwater reservoirs, Zamrsky et al. (2020) showed that the topographic profile of the shelf is a key characteristic governing the emplacement of freshwater in the system. These findings together suggest that localized topographic variations on the seafloor should be considered as important features, with a high likelihood to coincide with OFG in regions where the appropriate paleo-hydrologic conditions existed.

The extent of freshwater recharge varies across the four well sites. The sediment column in the most proximal part of the model near the projected location of well 6011 is completely freshened in every scenario. Most of the sediment column in the region of M27 is freshened, with brackish pore fluid remaining below 400 m in the well. The salinity distribution at the end of the recharge phase indicate that freshening occurs by top-down as well as lateral flow of freshwater from the landward direction. At site M28 and M29, freshening occurs down to a maximum of 300 m, the deeper sediments remain relatively saline across all scenarios. Freshening in this region appears to primarily occur by top-down meteoric recharge via surface-connected pathways. The model shows that the LGM is not sufficient to freshen the deeper reservoirs that have been observed at sites M27 and M28. The deep freshwater intervals at those wells are either relics of a previous interglacial period, or recharge via 3D flow pathways not captured in this study.

783 The offshore extent of freshening in our model is consistent with an earlier regional numerical
784 study of the Pleistocene glacial maximum on the US Atlantic margin by Cohen et al. (2010). That
785 study also reported freshwater emplacement at distances up to 100 km from the modern-day
786 coastline. They attributed this to offshore directed flow in shallow outcropping Miocene sands.
787 The layered regional model considered by Cohen et al. (2010) did not account for the presence of
788 discontinuities in confining layers. The lateral heterogeneity in our model captures this important
789 component of the recharge process, highlighting the importance of incorporating realistic
790 geological features when characterizing OFG systems. Recharge is not strictly confined to the
791 inland outcrops of sandy units, rather it occurs all across the shelf transect driven by the
792 topographic gradient and controlled by the sequence stratigraphic architecture. Our simulations
793 consider both low- and high onshore – offshore connectivity scenarios. These clearly show that
794 in the presence of geological heterogeneity, offshore-directed flow does not translate to increased
795 freshwater emplacement in the distal shelf region. This implies that offshore-directed flow, due to
796 terrestrial drivers such as over-pressure induced by ice-sheet loading, are not an absolute
797 requirement for emplacement of freshwater in sediments that are currently far offshore.

798 Previous numerical studies showed that increased advective forces which drive sub-glacial
799 freshwater emplacement do not extend far beyond the edge of the ice sheet (Cohen et al. 2010;
800 Siegel et al. 2014). Results obtained on this New Jersey transect of enhanced terrestrial discharge
801 are consistent with this dynamic system behavior. An elevated hydraulic head at the inland
802 boundary only affected the salinity observed in the proximal part of the model, while the overall
803 emplaced volume of freshwater increased only marginally in response to an increased hydraulic
804 head of 25 m at the inland boundary. This value was chosen to represent a high end member value
805 of enhanced terrestrial discharge based on regional reconstructions presented in Cohen et al.
806 (2010), which showed elevated heads of 30 m – 40 m during the Pleistocene lowstand in the region
807 onshore New Jersey shelf. This constant head value represents an estimate of potential offshore
808 directed flow. Actual values of offshore groundwater discharge are irregular and vary with time
809 (Burnett et al. 2006).

810 The most significant change in the volume of freshwater occurred when anisotropic permeability
811 was implemented. An anisotropic ratio of ten resulted in an observable change in the shape of the
812 freshwater – saltwater interface. These results suggests that the downward percolation of

freshwater into the sediment column via surface connected pathways is a crucial mechanism for freshwater emplacement. Notably, the reduction in freshwater recharge was smaller in the HC model. This we attribute to the higher lateral connectivity relative to the LC model, which allows more freshwater into the sediments. However, in the case of higher anisotropy both models result in similar volumes of recharge. This highlights again the importance of surface derived recharge. Meisler et al. (1984) found that a lower anisotropy ratio resulted in a landward as well as downward shift of the sharp interface position in their layered shelf model. This basic correlation is observed in our results; however, the response is considerably more dynamic in the heterogeneous shelf model. The implementation of a low anisotropy ratio of two, resulted in a closer fit to the observed data. This suggests that the system can be characterized by low to moderate permeability anisotropy. Our study highlights the importance of constraining permeability anisotropy in the characterization of OFG systems. Anisotropy can be identified via specialized laboratory measurements on core plugs (Crawford et al. 2008). Such an approach can improve model constraints. However, upscaling to the field scale is a non-trivial part of incorporating this information into flow models, which is dependent on the geological heterogeneity (Menke et al. 2021; Szymkiewicz 2013)

In the layered depositional setting of the New Jersey shelf, density instabilities occur as freshwater is driven oceanward and advances non-uniformly. Preferential flow in high-permeability intervals creates a complex combination of advective and diffusive processes during the lowstand period. We found two key mechanisms of freshening. The primary mechanism is advective freshening driven by the oceanward hydraulic gradient. This causes freshwater to flow preferentially into high-permeability sediment layers, flushing out the salt water. Density instabilities occur where aquifer units are freshened while overlying confining units remain saturated with denser saline pore fluid for a longer period. In the early stages of recharge, this juxtaposition results in sharp salinity contrasts between aquifers and overlying confining units. This contrast gives way to the secondary mechanism, convective mixing, resulting from the unstable concentration gradients in the layered sedimentary setting. Denser saline pore fluid in confining layers fingers downward into freshened intervals, while more buoyant freshwater migrates upward. The temperature gradient on the shelf likely contributes to the buoyancy of freshwater driven deeper into the sediment column.

4.2 Marine transgression and freshwater survival

Kooi et al. (2000) conducted a numerical study analyzing the various modes by which seawater intrusion occurs during a marine transgression. Their study identified four modes: (1) horizontal intrusion in the case of a slow transgression, (2) vertical intrusion by seawater fingering during rapid transgression over a highly permeable medium, (3) vertical intrusion by diffusion for rapid transgressions over a low-permeability medium, and (4) vertical intrusion by a combination of diffusion and low-salinity fingering for rapid transgression over a layered subsurface. Kooi et al. (2000) showed that there is a critical rate of marine transgression that determines whether a transition occurs from horizontal to one of the vertical intrusion modes. The marine transgression that took place after the last glacial maximum can be considered as above critical for the low-angle New Jersey shelf. The 161 km model domain proceeded from sub-aerial exposure to complete inundation with ocean water in approximately 12 000 years from the LGM to the present day. This corresponds to a transgression rate of approximately 13 m per year. Based on the results obtained in this study, there is evidence for three vertical modes of intrusion associated with the rapid transgression. In the distal region of the shelf, where low-permeability facies are dominant, a seaward dipping wedge of low-salinity pore fluid develops during the transgression. In the mid-shelf region, low-permeability intervals near the ocean floor preserve a substantial amount of fresh water, however, downward fingering of saline fluid through overlying shales create lateral salinity variations in the reservoir (R3). This results in a broad and relatively well-mixed transition zone on the oceanward end of this reservoir. The landward part of R3 is characterized by sharp boundaries between freshwater intervals and saline pore fluid in overlying confining layers (see Fig. 17). In the more proximal region of the shelf, the permeability distribution trends towards more high-permeability sands, where a different mode can be observed. This mode is characterized by downward fingering ocean water creating a high-salinity pore fluid columns, which compartmentalize the surviving freshwater body (Fig. 17 and 18). A field study of vertical seawater intrusion on a freshwater lens by Post and Houben (2017) showed that downward fingering of saline pore fluid was the dominant driver of mixing. Groen et al. (2000) showed how this downward fingering process can speed up the salinization of sequestered freshwater on the continental shelf. Our stochastic New Jersey shelf model accounts for discontinuities in the overlying confining units, and thus highlights the importance of geological heterogeneity on the survival of offshore freshened groundwater. Future numerical studies, for example in 3D, can

benefit from considering the various modes of intrusion that generated by the subsurface heterogeneity and underlying regional permeability trends. The 2D approach presented in this study does not account for all potential flow pathways.

The present-day scenario consisting of a layered and compartmentalized fresh-brackish water zone results from connected pathways between the ocean and deeper, permeable sediments. Along these pathways, density-driven flow salinifies most permeable units, while cemented and low-permeability intervals shield some freshwater reservoirs from above. These findings support the salinification mechanisms suggested by Lofi et al. (2013) for mid-shelf reservoirs based on a qualitative shelf model. These authors postulated that either outcropping reservoirs at the seafloor, or a pathway of intermediary connected reservoirs could explain the salinization of the mid-shelf region. Our numerical simulations favor the latter of these two explanations. Lateral heterogeneity results in complex, connected pathways between the ocean and deeper reservoirs of emplaced freshwater. This is consistent with earlier simulations of surviving freshwater body in a heterogeneous shelf model presented by Thomas et al. (2019), in which authors showed that the observed salinity distribution is strongly influenced by the stratigraphic architecture. As we address this problem only in 2D, the full complexity and influence of such pathways cannot be entirely captured. In a 3D model, ocean water can enter reservoirs from multiple directions, resulting in different survival rates for freshened reservoirs. However, considering that depositional environment for Miocene sediments has been identified as wave-dominated (Monteverde et al. 2008; Proust et al. 2018), we postulate that the complexity of the groundwater flow and solute transport on New Jersey shelf is largely a function of dip-oriented variation in sediment properties. Based on the principles of a wave-dominated environment, it can be assumed that there is considerably less variation in sediment properties in the shoreline parallel direction. The 2D model thus provides a representative perspective on the dynamic life cycle of offshore freshened groundwater in the New Jersey passive margin setting.

4.3 Modern or Fossil Water?

The results of our numerical study can be discussed in the light of the two main hypotheses proposed for explaining the presence of freshwater offshore New Jersey. The first hypothesis identifies the source as meteoric and sub-ice-sheet recharge during the sea-level lowstand

associated with the last glacial maximum or potentially earlier periods (Cohen et al. 2010; Kooi and Groen 2001; Person et al. 2003; Siegel et al. 2014). Results presented in this study show that both high- and low-permeability sediments of the New Jersey shelf were flushed with freshwater during the LGM in all scenarios considered. At the expedition 313 well sites in the mid-shelf region, we observed freshening of the shallow reservoirs, consistent with present-day observations. However, deeper reservoirs in M27 and M28 remained relatively saline during the simulated period. In the subsequent transgressive period, these reservoirs underwent partial salinification, but a significant portion of fresh – brackish water survives to the present day. This observation supports the hypothesis that freshwater sampled at Expedition 313 sites would be fossil water emplaced via meteoric recharge during the LGM. Our simulations suggest that the deeper reservoirs in M27 and M28 may even pre-date the LGM. An alternative explanation for these reservoirs is that they were recharged via shoreline parallel connected flow pathways, which our 2D model does not capture. It is plausible that a full 3D characterization of the shelf would result in the freshening of these deeper reservoirs during the LGM.

To date there have been no published studies on the absolute ages of groundwater sampled at the Expedition 313 sites. In an earlier coastal aquifer study, McAuley et al. (2001) analysed radioactive isotopes in four wells in order to estimate groundwater ages in the coastal Atlantic City 800-foot sand, the principal source of water supply for southern New Jersey coastal communities. Their transect extended from inland to approximately 8.5 km offshore. At the Pleasantville well site, 1.6 km inland of the coastline, sampled water was dated at 17 950 years BP. The two offshore sites yielded ages of at least 22 000 years BP and possibly older than 30 000 years BP. These dates support the hypothesis of Pleistocene freshwater emplaced in the mid-shelf reservoirs. As a caveat, van Geldern et al. (2013) reasoned that these dates may be over-estimated, as it cannot be verified whether the relevant correction models were used in the calculation of the radiocarbon ages.

Despite not providing information on absolute ages, stable isotope ratios of oxygen and hydrogen in water were used as natural tracers to characterize the origins and composition in both marine and terrestrial studies (Bigg and Rohling 2000; Bowen and Wilkinson 2002; Dutton et al. 2005; Maslin and Swann 2006). van Geldern et al. (2013) analysed the stable isotope composition of Expedition 313 samples. They concluded that the freshwater was either of modern meteoric origin and therefore rapidly recharged, or it pre-dates the Pleistocene and had been recharged during a

period with similar climatic conditions to modern times. $\delta^{18}O$ values of water sampled at Expedition 313 sites range between -0.8 ‰ and -7.0 ‰, indicating a mixture of modern meteoric recharge and seawater as the source of pore fluids (van Geldern et al. 2013). Water of Pleistocene age would normally be characterized by a comparatively lower range of isotope values (Mook and Rozanski 2000): $\delta^{18}O$ values in the range of -11 ‰ to -18.0 ‰ were reported for Pleistocene-age recharge in the Cambrian-Ordovician aquifer of Iowa, further inland on the North American continent (Siegel 1991). However, an isotopically depleted body of Pleistocene water was shown there to be caused by a dilution of a combination of glacial meltwater and precipitation. This diluted water mass was deep in the aquifer, below 300 m of confining layers, and $\delta^{18}O$ values are within the range of modern precipitation for Iowa (from –11 to –6.0 ‰) (Siegel 1991). This regional setting of the sample locations analysed by Siegel (1991., Fig. 2) is analogous to the New Jersey case, which had not been covered by ice-sheets as it was rather proximal to the edges of their southern-most advance (Cohen et al. 2010). The depleted isotopic signature of the Pleistocene groundwater suggests that the climate at the end of the last glacial period was mild. This conclusion is also supported in multi-disciplinary studies (Hanshaw et al. 1979; Morgan et al. 1987). These studies provide strong evidence that groundwater isotope values similar to that of modern precipitation do not unambiguously indicate recent recharge.

Our simulation results do not support any significant role of modern recharge in the persistence of the mid-shelf freshwater system observed by IODP Expedition 313 (Mountain et al. 2010). Previous studies have shown that in certain geological settings, an active recharge of offshore freshened groundwater reservoirs can occur (Michael et al. 2016; Varma and Michael 2012). Our stochastic approach considered both high and low onshore-offshore connectivity scenarios and found only marginal changes in present-day freshwater distrbutions at the most proximal regions of the model domain (i.e., well site 6011). Observed profiles at IODP expedition 313 sites are unaffected by offshore directed discharge. A more speculative hypothesis suggests that the freshwater may date back to the Miocene age (Meisler et al. 1984). In a study of groundwater residence times in the Alberta Basin Gupta et al. (2015) performed simulations constrained by hydrogeologic and geochemical observations. The results showed dilution of old pore fluids occurred due to flushing by younger waters. The hydrogeologic model presented in this New Jersey study shows that significant flushing of the mid-Miocene sediments likely occurred during

962 the last glacial maximum. This exchange and mixing of pore fluid likely occurred in multiple
963 glacial – interglacial cycles and can therefore influence the age of pore fluid determined solely by
964 geochemical methods. Our numerical results strongly suggests that water emplaced before the
965 Pleistocene would have likely been flushed out since, and consequently, its signature would have
966 been over-printed by relatively younger groundwater, as speculated by Meisler et al. (1984).

967

968 The results of this study are broadly consistent with the salinity profiles of the multi-layered
969 reservoir system of offshore freshened groundwater observed in IODP Expedition 313 (Mountain
970 et al. 2010) and the projected position of AMCOR well site 6011. Portions of the surviving
971 freshwater in our numerical simulations are also consistent with the resistivity anomalies identified
972 by an independently conducted electromagnetic survey of the US continental shelf by Gustafson
973 et al. (2019). In the proximal region of the shelf, Gustafson et al. (2019) considered the strong
974 resistivity anomaly as evidence for an active connection between onshore and offshore freshwater
975 reservoirs. However, numerical simulations show that offshore directed only influences the
976 freshwater in the most proximal region of the model (i.e., within 20 km from the landward
977 boundary). Downward fingering ocean water compartmentalizes the surviving freshwater system
978 into isolated, hydraulically disconnected pockets as discussed earlier. In both high and low
979 onshore-offshore connectivity scenarios, the offshore directed discharge is insufficient to maintain
980 open freshwater conduits to the surviving reservoirs in the mid-shelf region. Figure 20 shows a
981 visual comparison between the resistivity anomaly and our paleo-reconstruction on both high and
982 low connectivity model scenarios. Our model domain was clipped, and color scales were adjusted
983 to match the presented resistivity data. There is a reasonably close fit between the resistivity
984 anomalies and the simulated freshwater distribution. The proximal body of freshwater preserved
985 in our model is consistent with the seaward dipping resistivity anomaly presented by Gustafson et
986 al. (2019). However, our heterogeneous model domain captures lateral variability in pore fluid
987 concentration resulting from downward fingering via seafloor-connected pathways. This
988 downward fingering is more pronounced in the high onshore-offhshore connectivity model, as it
989 features thicker high permeability intervals that more readily facilitate downward fingering. A
990 numerical study of aquifer vulnerability to ocean storm surges by Cardenas et al. (2015) found that
991 while zones of downward fingering saline pore fluid were apparent in their numerical model
992 results, there was only tentative evidence of their existence in the geophysical field measurements.

Electromagnetic methods integrate resistivity over volumes which become larger with increasing depth. Therefore, small-scale signatures at greater depth, such as the saline fingers are not resolved. Finally, the shallow anomaly in the mid-shelf region, which gradually fades in the oceanward direction is similar to the preserved freshwater reservoir earlier described as R3. This reservoir has the lowest salinity in the region of M29 and gradually becomes more saline in the oceanward direction, consistent with the trend of the anomaly.

Figure 20 shows a qualitative comparison between independent datasets. Future studies can benefit from integrating numerical flow simulations into a process-based inversion scheme to improve constraints of subsurface properties such as hydraulic conductivity or porosity (Wagner and Uhlemann 2021). A stochastic approach to capture geological heterogeneity, as presented in this paper, can produce more geologically representative constraints on porosity distribution, which strongly influences the interpretation of resistivity data. Additionally, structurally constrained inversion can integrate known stratigraphic features, such as cemented intervals, into geophysical data processing as detailed by Wagner and Uhlemann (2021).

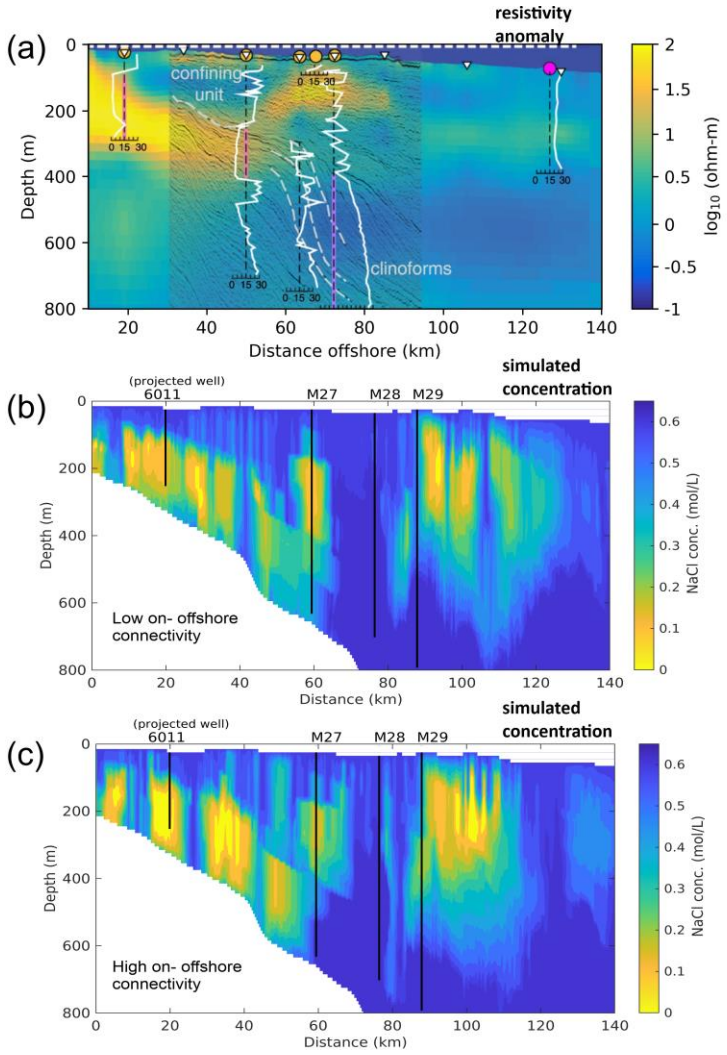

Figure 20 Visual comparison of resistivity anomaly reporty by Gustafson et al. (2019) and numerical simulation results of our paleo-hydrological reconstruction of the LGM on the New Jersey shelf. (b) and (c) show the low and high onshore – offshore connectivity scenarios, respectively. Both results show freshwater distribution that is broadly consistent with the observed resistivity anomaly. Future studies can benefit from joint or process based inversion of resistivity data to better constrain the characterization of OFG systems.

Based on the evidence of this numerical study, and previous findings discussed earlier, we conclude that the freshwater system had been almost completely recharged during the lowstand period associated with the last glacial maximum beginning at least 70 000 years ago. Although not studied here, it can also be safely assumed that some partial recharge into the sediments also occurred prior to 70 000 years ago. Therefore, the observed freshwater system is slowly shrinking due to diffusion and density-driven flow through connected pathways to the ocean. This observation does not account for the 3D effects of laterally connected pathways that can likely alter the observed distribution. The net increase in freshwater stored on the New Jersey shelf over the simulated period suggest that the cyclical flushing and re-salinization of shelf sediments, which

takes place over glacial – interglacial cycles is an asymmetrical process. This means that some portion of the freshwater recharged into the system during glacial sea-level lowstands will likely survive the typical inter-glacial period and thus the system favours storage of freshened pore fluid over geological time-scales. A numerical study of freshwater survival on the New Jersey shelf by Thomas et al. (2019) also found that at least 15 % of initially assumed freshwater volume had survived after simulating 30 000 years of ocean coverage.

4.4 Resource perspective

We present some simple back-of-the-envelope calculations based on the paleo-reconstruction presented in this study. The volume of freshwater in this case was approximately 0.54 km^3. The model cell width of 100 m means this can be expressed as a potential storage of 5.4 km^3 of fresh-to-brackish water per kilometer of the New Jersey coastline. This is more than a previous estimate of 3.8 km^3 of freshened groundwater per kilometer of coastline presented in a study by Cohen et al. (2010), which was an average value based on data from four different continental shelf transects. The value presented by Cohen et al. (2010) is based on an effective sediment porosity of 20 %. The estimate presented in this study is directly related to the New Jersey case of relatively unconsolidated sediments on a passive margin setting, with porosity ranging from 40 % to 60 %. Extrapolating these results along 180 km of the New Jersey coastline, we estimate about 1 000 km^3 of fresh to brackish water to exist under present-day conditions on the shelf. A comparable value of 1 300 km^3 of freshwater was estimated to be sequestered in continental shelf reservoirs in New England, US (Cohen et al. 2010). To put this into perspective, the daily groundwater water extraction in entire United States, was estimated at 73 km^3 in 2010 , based on an extraction rate of 0.2 km^3 / day (Maupin et al. 2014).

The New Jersey shelf is only one of several occurrences of extensive systems of offshore freshened groundwater (Micallef et al. 2020a). As the understanding of these systems continues to expand, an important next step is the characterization of offshore fresh groundwater reservoirs. The results of this study on a representative geological model highlight the complex and dynamic interplay of topography, sediment heterogeneity, and anisotropy of permeability. These factors appear to have systemic effects on the volume of freshwater emplaced during low-stand periods as well as the survival and storage of this freshwater during subsequent transgressive periods. The

characterization of offshore freshened groundwater requires dedicated hydrogeological data acquisition and analysis for deciphering the complex history of these reserves and characterizing their resource potential.

5 Conclusions

Integrating realistic heterogeneity based on seismic and well data can explain the multi-layered freshwater system on the New Jersey shelf. A geologically representative model shows that the OFG system is laterally compartmentalized by downward fingering saline fluids through connected pathways to the ocean. This shows that the accurate modelling of offshore fresh groundwater reservoirs requires adequate characterization of the geological heterogeneity. Our sensitivity analysis shows surface derived meteoric recharge is the primary mechanism for freshening of the sediment column during sealevel lowstand. Surface connected pathways and permeability anisotropy are therefore fundamental characteristics of the New Jersey shelf OFG system.

By using a stochastic modeling approach to generate high and low onshore-offshore connectivity scenarios, we show that terrestrial discharge is not responsible for the freshwater intervals observed at Expeditions 313 well sites. Meteoric recharge during the lowstand associated with the LGM can sufficiently explain the existence of shallow reservoirs (< 400 mbsf). The emplacement of freshwater was driven primarily by the topographic gradient, which caused surface recharge to infiltrate the oceanward-dipping sediments. Deeper freshened intervals at wells sites M27 and M28 are either relics of a previous interglacial period, or were recharged via 3D flow pathways not captured in this study. However, the increasing salinity with depth is not consistent with a deeper freshwater source.

Finally, the observed volumetric trends suggest that the cyclical flushing and re-salinization of shelf sediments that takes place over glacial – interglacial cycles is an asymmetrical process, which favours storage of freshened pore fluid. In light of present-day stressed water supply and changing climate conditions, this has implications for the consideration of these unconventional groundwater resources. While our estimates of the freshwater volume stored on the New Jersey shelf qualifies them as a potential resource, it is important to note that these reserves are stored in low-permeability intervals and are slowly shrinking due to salinization.

Acknowledgments and Data

Simulations were performed with computing resources granted by RWTH Aachen University under project rwth0761.

Funding for this project is provided by the Deutsche Forschungsgemeinschaft (DFG) within the Priority Programme 527 – "International Ocean Discovery Program" (IODP) under grant RE-3863/2-

Directions to access to the algorithm used to generate the results in this study (SHEMAT-Suite) is available in the in-text data citation reference: Keller et al. (2020). This software is open source.

References

Austin J. A., Christie-Blick N., Malone M. J. (1998) Proc. ODP, Init. Rpts, 174A, College Station, TX (Ocean Drilling Program), doi: 10.2973/odp.proc.ir.174a.1998.

Bigg G. R., Rohling E. J. (2000) An oxygen isotope data set for marine waters, Journal of Geophysical Research 105(C4):8527–8535.

Bowen G. J., Wilkinson B. (2002) Spatial distribution of δ18O in meteoric precipitation, Geology 30(4):315, doi: 10.1130/0091-7613(2002)030<0315:SDOOIM>2.0.CO;2.

Burnett W. C., Aggarwal P. K., Aureli A., Bokuniewicz H., Cable J. E., Charette M. A., Kontar E., Krupa S. et al. (2006) Quantifying submarine groundwater discharge in the coastal zone via multiple methods, The Science of the total environment 367(2-3):498–543, doi: 10.1016/j.scitotenv.2006.05.009.

Cardenas M. B., Bennett P. C., Zamora P. B., Befus K. M., Rodolfo R. S., Cabria H. B., Lapus M. R. (2015) Devastation of aquifers from tsunami-like storm surge by Supertyphoon Haiyan, Geophysical Research Letters 42(8):2844–2851, doi: 10.1002/2015GL063418.

Clauser C (2003) Numerical simulation of reactive flow in hot aquifers using SHEMAT and Processing SHEMAT. Springer, Berlin.

1105 Cohen D., Person M., Wang P., Gable C. W., Hutchinson D., Marksamer A., Dugan B., Kooi H.
1106 et al. (2010) Origin and extent of fresh paleowaters on the Atlantic continental shelf, USA,
1107 Groundwater 48(1):143–158.

1108 Crawford B. R., Webb D. W., Searles K. H. (2008) Plastic Compaction and Anisotropic
1109 Permeability Development in Unconsolidated Sands with Implications for Horizontal Well
1110 Performance. In The 42nd U.S. Rock Mechanics Symposium (USRMS). American Rock
1111 Mechanics Association, San Francisco, California.

1112 Deutsch CV, Pyrcz M (2014) Geostatistical reservoir modeling. Second edition / Michael J. Pyrcz,
1113 Clayton V. Deutsch. Oxford University Press, Oxford.

1114 Dutton A., Wilkinson B. H., Welker J. M., Bowen G. J., Lohmann K. C. (2005) Spatial distribution
1115 and seasonal variation in 18 O/ 16 O of modern precipitation and river water across the
1116 conterminous USA, Hydrological Processes 19(20):4121–4146, doi: 10.1002/hyp.5876.

1117 Freeze RA, Cherry JA (1979) Groundwater. Prentice Hall, Englewood Cliffs, NJ.

1118 Gelhar L. W., Welty C., Rehfeldt K. R. (1992) A critical review of data on field-scale dispersion
1119 in aquifers, Water Resources Research 28(7):1955–1974, doi: 10.1029/92WR00607.

1120 Groen J., Velstra J., Meesters A.G.C.A. (2000) Salinization processes in paleowaters in coastal
1121 sediments of Suriname: evidence from \textdelta 37Cl analysis and diffusion modelling,
1122 Journal of Hydrology 234(1-2):1–20, doi: 10.1016/S0022-1694(00)00235-3.

1123 Gupta I., Wilson A. M., Rostron B. J. (2015) Groundwater age, brine migration, and large-scale
1124 solute transport in the Alberta Basin, Canada, Geofluids 15(4):608–620, doi:
1125 10.1111/gfl.12131.

1126 Gustafson C., Key K., Evans R. L. (2019) Aquifer systems extending far offshore on the U.S.
1127 Atlantic margin, Scientific reports 9(1):8709, doi: 10.1038/s41598-019-44611-7.

1128 Hampson G. J. (2010) Sediment dispersal and quantitative stratigraphic architecture across an
1129 ancient shelf, Sedimentology 57(1):96–141, doi: 10.1111/j.1365-3091.2009.01093.x.

1130 Hanshaw B. B., Winograd I. J., Pearson F. J., Jacoby G. C. (1979) Stable isotope studies of
1131 subglacially precipitated carbonates and of ancient ground water: Paleoclimatic
1132 implications. In Gordon Jacoby (ed.)Proceedings of International Meeting on Stable
1133 Isotopes in Tree-Ring Research. Lamont-Doherty, Geological Observatory, Columbia
1134 University New York, New Paltz, New York:102–104.

1135 Hastie T, Tibshirani R, Friedman JH (2009) The elements of statistical learningData mining,
1136 inference, and prediction / Trevor Hastie, Robert Tibshirani, Jerome Friedman. 2nd ed.
1137 Springer, New York (Springer series in statistics).

1138 Hathaway J. C., Poag C. W., Valent P. C., Miller R. E., Schultz D. M., Manhe F. T., Kohout F. A.,
1139 Bothner M. H. et al. (1979) US Geological Survey Core Drilling on the Atlantic Shelf,
1140 Science 206(4418):515–527.

1141 Hill MC, Tiedeman CR (2006) Effective Groundwater Model CalibrationWith Analysis of Data,
1142 Sensitivities, Predictions, and Uncertainty. John Wiley & Sons.

1143 Hobbs B., Ord A. (2015) Fluid Flow. In BE Hobbs, Ord, Alison (eds.)Structural geology. The
1144 Mechanics of Deforming Metamorphic Rocks. Elsevier, Amsterdam, Netherlands:365–
1145 421.

1146 Holcomb D. J., Olsson W. A. (2003) Compaction localization and fluid flow, Journal of
1147 Geophysical Research 108(B6), doi: 10.1029/2001JB000813.

1148 Imbrie J., Hays J. D., Martinson D. G., McIntyre A., Mix A. C., Morley J. J., Pisias N. G., Prell
1149 W. L. et al. (1984) The orbital theory of Pleistocene climate: support from a revised
1150 chronology of the marine d18O record. In A Berger (ed.)Milankovitch and Climate, Part
1151 1. D. Reidel Publishing Company, Boston, MA.

1152 Jazayeri A., Werner A. D. (2019) Boundary Condition Nomenclature Confusion in Groundwater
1153 Flow Modeling, Ground Water 57(5):664–668, doi: 10.1111/gwat.12893.

1154 Johnsen S. J., Dahl-Jensen D., Dansgaard W., Gundestrup N. (1995) Greenland
1155 palaeotemperatures derived from GRIP bore hole temperature and ice core isotope profiles,
1156 Tellus B 47(5):624–629, doi: 10.1034/j.1600-0889.47.issue5.9.x.

1157 Johnston R. H. (1983) The saltwater-freshwater interface in the Tertiary limestone aquifer,
1158 southeast Atlantic outer-continental shelf of the U.S.A, Journal of Hydrology 61(1-3):239–
1159 249, doi: 10.1016/0022-1694(83)90251-2.

1160 Keller J., Rath V., Bruckmann J., Mottaghy D., Clauser C., Wolf A., Seidler R., Bücker H. M. et
1161 al. (2020) SHEMAT-Suite: An open-source code for simulating flow, heat and species
1162 transport in porous media, SoftwareX 12:100533, doi: 10.1016/j.softx.2020.100533.

1163 Kooi H., Groen J. (2001) Offshore continuation of coastal groundwater systems; predictions using
1164 sharp-interface approximations and variable-density flow modelling, Journal of Hydrology
1165 246(1):19–35.

1166 Kooi H., Groen J., Leijnse A. (2000) Modes of seawater intrusion during transgressions, Water
1167 Resources Research 36(12):3581–3589, doi: 10.1029/2000WR900243.

1168 Labourdette R., Hegre J., Imbert P., Insalaco E. (2008) Reservoir-scale 3D sedimentary modelling:
1169 approaches to integrate sedimentology into a reservoir characterization workflow,
1170 Geological Society, London, Special Publications 309(1):75–85, doi: 10.1144/SP309.6.

1171 Lachenbruch A., Sass J. H. (1977) Heat flow from the crust of the United States and the Thermal
1172 Regime of the Crust. In Heacock JG, Keller GV, Oliver JE, Simmons G (eds.)The Earth's
1173 Crust, vol. 20. American Geophysical Union, Washington:p 635–675.

1174 Lofi J., Inwood J., Proust J.-N., Monteverde D. H., Loggia D., Basile C., Otsuka H., Hayashi T. et
1175 al. (2013) Fresh-water and salt-water distribution in passive margin sediments: Insights
1176 from Integrated Ocean Drilling Program Expedition 313 on the New Jersey Margin,
1177 Geosphere 9(4):1009–1024.

1178 Malone M. J., Claypool G., Martin J. B., Dickens G. R. (2002) Variable methane fluxes in shallow
1179 marine systems over geologic time: The composition and origin of pore waters and
1180 authigenic carbonates on the New Jersey shelf, Marine Geology 189(3):175–196.

1181 Manahan SE (2011) Fundamentals of Environmental Chemistry, Third Edition. CRC Press.

1182 Maslin M. A., Swann G. E.A. (2006) Isotopes in Marine Sediments. In MJ Leng (ed.)Isotopes in
1183 Palaeoenvironmental Research. Developments in paleoenvironmental research, vol. 10.
1184 Springer, Dordrecht.

1185 Maupin M. A., Kenny J. F., Hutson S. S., Lovelace J. K., Barber N. L., Linsey K. S. (2014)
1186 Estimated use of water in the United States in 2010 Circular, doi: 10.3133/cir1405.

1187 McAuley S. D., Barringer J. L., Paulachok G. N., Clark J. S., Zapecza O. S. (2001) Groundwater
1188 flow and quality in the Atlantic City 800 foot Sand, New Jersey, Geological Survey Report
1189 GSR 41, Trenton, NJ, doi: 10.7282/T38913ZV.

1190 Meisler H., Leahy P. P., Knobel L. L. (1984) Effect of eustatic sea-level changes on saltwater-
1191 freshwater in the northern Atlantic Coastal Plain, US Geological Survey Water-Supply
1192 Paper 2255, Alexandria, VA.

1193 Menke H. P., Maes J., Geiger S. (2021) Upscaling the porosity-permeability relationship of a
1194 microporous carbonate for Darcy-scale flow with machine learning, Scientific Reports
1195 11(1):2625, doi: 10.1038/s41598-021-82029-2

1196 Micallef A., Person M., Berndt C., Bertoni C., Cohen D., Dugan B., Evans R., Haroon A. et al.
1197 (2020a) Offshore freshened groundwater in continental margins, Reviews of Geophysics,
1198 doi: 10.1029/2020RG000706.

1199 Micallef A., Person M., Haroon A., Weymer B. A., Jegen M., Schwalenberg K., Faghih Z., Duan
1200 S. et al. (2020b) 3D characterisation and quantification of an offshore freshened
1201 groundwater system in the Canterbury Bight, Nature Communications 11(1):1372, doi:
1202 10.1038/s41467-020-14770-7.

1203 Miller K. G., Browning J. V., Mountain G. S., Bassetti M. A., Monteverde D., Katz M. E., Inwood
1204 J., Lofi J. et al. (2013) Sequence boundaries are impedance contrasts: Core-seismic-log
1205 integration of Oligocene-Miocene sequences, New Jersey shallow shelf, Geosphere
1206 9(5):1257–1285.

1207 Miller K. G., Snyder S. W. (1997) Island Beach, Atlantic City, and Cape May Sites, New Jersey
1208 Coastal Plain, Proceedings of the Ocean Drilling Program, Scientific Results, 150X,
1209 College Station, TX (Ocean Drilling Program), doi: 10.2973/odp.proc.ir.150X.1994.

1210 Miller K. G., Sugarman P., van Fossen M., Liu C., Browning J. V., Queen D., Aubry M.-P.,
1211 Burckle L. D. et al. (1994) Island Beach Site Report. In: Miller KG et al.(eds) Proc. ODP,
1212 Init. Rpts., 150X, College Station, TX (Ocean Drilling Program), doi:
1213 10.2973/odp.proc.ir.150x.111.1994.

1214 Monteverde D. H., Mountain G. S., Miller K. G. (2008) Early Miocene sequence development
1215 across the New Jersey margin, Basin Research 20(2):249–267.

1216 Mook W., Rozanski K. (2000) Environmental isotopes in the hydrological cycle, IAEA Publish
1217 39.

1218 Morgan A. V., Ruddiman W. F., Wright H. E. (1987) Late Wisconsin and early Holocene
1219 paleoenvironments of east-central North America based on assemblages of fossil
1220 Coleoptera, The Geology of North America 3:353–370.

1221 Mountain G., Proust J. N., McInroy D., Cotterill C., Expedition 313 Scientists (2010) Proc. IODP,
1222 313. Integrated Ocean Drilling Program Management International, Inc., Tokyo, doi:
1223 10.2204/iodp.proc.313.2010.

1224 O.S.P.O. (2013) Sea Surface Temperature Contour Charts (NOAA Office of Satellite and Product
1225 Opertations), https://www.ospo.noaa.gov/Products/ocean/sst/contour/, checked on
1226 1/2/2018.

1227 Paldor A., Aharonov E., Katz O. (2020) Thermo-haline circulations in subsea confined aquifers
1228 produce saline, steady-state deep submarine groundwater discharge, Journal of Hydrology
1229 580:124276, doi: 10.1016/j.jhydrol.2019.124276.

1230 Person M., Dugan B., Swenson J. B., Urbano L., Stott C., Taylor J., Willett M. (2003) Pleistocene
1231 hydrogeology of the Atlantic continental shelf, New England, Geological Society of
1232 America Bulletin 115(11):1324–1343.

1233 Pope DA, Gordon AD (1999) Simulation of Ground-water Flow and Movement of the Freshwater-
1234 saltwater Interface in the New Jersey Coastal Plain. U.S. Department of the Interior, U.S.
1235 Geological Survey.

1236 Post V. E., Groen J., Kooi H., Person M., Ge S., Edmunds W. M. (2013) Offshore fresh
1237 groundwater reserves as a global phenomenon, Nature 504(7478):71–78.

1238 Proust J.-N., Pouderoux H., Ando H., Hesselbo S. P., Hodgson D. M., Lofi J., Rabineau M.,
1239 Sugarman P. J. (2018) Facies architecture of Miocene subaqueous clinothems of the New
1240 Jersey passive margin: Results from IODP-ICDP Expedition 313, Geosphere 14(4).

1241 Ramires M. L., Nieto de Castro C. A., Nagasaka Y., Nagashima A., Assael M. J., Wakeham W.
1242 A. (1995) Standard Reference Data for the Thermal Conductivity of Water, Journal of
1243 Physical and Chemical Reference Data 24(3):1377–1381, doi: 10.1063/1.555963.

1244 Rath V., Wolf A., Bücker H. M. (2006) Joint three-dimensional inversion of coupled groundwater
1245 flow and heat transfer based on automatic differentiation: sensitivity calculation,
1246 verification, and synthetic examples, Geophysical Journal International 167(1):453–466.

1247 Reynolds A. D. (1999) Dimensions of Paralic Sandstone Bodies, AAPG Bulletin 83
1248 (1999)(2):211–229, doi: 10.1306/00AA9A48-1730-11D7-8645000102C1865D.

1249 Riedel M., Reiche S., Aßhoff K., Buske S. (2018) Seismic depth imaging of sequence boundaries
1250 beneath the New Jersey shelf, Marine Geophysical Research:1–16, doi: 10.1007/s11001-
1251 018-9360-9.

1252 Rubin H., Roth C. (1979) On the growth of instabilities in groundwater due to temperature and
1253 salinity gradients, Advances in Water Resources 2:69–76, doi: 10.1016/0309-
1254 1708(79)90013-7.

1255 Ryan W. B., Carbotte S. M., Coplan J. O., O'Hara S., Melkonian A., Arko R., Weissel R. A.,
1256 Ferrini V. et al. (2009) Global Multi-Resolution Topography synthesis, Geochemistry,
1257 Geophysics, Geosystems 10(3):n/a-n/a, doi: 10.1029/2008GC002332.

1258 Seifert D., Jensen J. L. (1999) Using sequential indicator simulation as a tool in reservoir
1259 description: issues and uncertainties, Mathematical Geology 31(5):527–550.

1260 Selley, RC, Sonnenberg, SA (eds.) (2015) Elements of petroleum geology. Third edition. Elsevier
1261 Academic Press is an imprint of Elsevier, Amsterdam, Boston.

1262 Siegel D. I. (1991) Evidence for dilution of deep, confined ground water by vertical recharge of
1263 isotopically heavy Pleistocene water, Geology 19(5):433, doi: 10.1130/0091-
1264 7613(1991)019<0433:EFDODC>2.3.CO;2.

1265 Siegel J., Person M., Dugan B., Cohen D., Lizarralde D., Gable C. (2014) Influence of late
1266 Pleistocene glaciations on the hydrogeology of the continental shelf offshore
1267 Massachusetts, USA, Geochemistry, Geophysics, Geosystems 15(12):4651–4670, doi:
1268 10.1002/2014GC005569.

1269 Simmons C. T., Fenstemaker T. R., Sharp J. M. (2001) Variable-density groundwater flow and
1270 solute transport in heterogeneous porous media: approaches, resolutions and future
1271 challenges, Journal of Contaminant Hydrology 52(1-4):245–275, doi: 10.1016/S0169-
1272 7722(01)00160-7.

1273 Szymkiewicz A. (2013) Upscaling from Darcy Scale to Field Scale. In A Szymkiewicz
1274 (ed.)Modelling Water Flow in Unsaturated Porous Media. Springer Berlin Heidelberg,
1275 Berlin, Heidelberg:139–175.

1276 Thomas A. T., Reiche S., Riedel M., Clauser C. (2019) The fate of submarine fresh groundwater
1277 reservoirs at the New Jersey shelf, USA, Hydrogeology Journal, doi: 10.1007/s10040-019-
1278 01997-y.

1279 Vajdova V., Baud P., Wong T.-f. (2004) Permeability evolution during localized deformation in
1280 Bentheim sandstone, Journal of Geophysical Research 109(B10), doi:
1281 10.1029/2003JB002942.

1282 Varma S., Michael K. (2012) Impact of multi-purpose aquifer utilisation on a variable-density
1283 groundwater flow system in the Gippsland Basin, Australia, Hydrogeology Journal
1284 20(1):119–134.

van Geldern R., Hayashi T., Böttcher M. E., Mottl M. J., Barth J. A., Stadler S. (2013) Stable isotope geochemistry of pore waters and marine sediments from the New Jersey shelf: Methane formation and fluid origin, Geosphere 9(1):96–112.

Wagner F. M., Uhlemann S. (2021) Chapter One - An overview of multimethod imaging approaches in environmental geophysics. In Cedric Schmelzbach (ed.)Inversion of Geophysical Data. Advances in Geophysics, vol. 62. Elsevier, The Netherlands:1–72.

Zamrsky D., Karssenberg M. E., Cohen K. M., Bierkens M. F., Oude Essink G. H. (2020) Geological Heterogeneity of Coastal Unconsolidated Groundwater Systems Worldwide and Its Influence on Offshore Fresh Groundwater Occurrence, Frontiers in Earth Science 7:2844, doi: 10.3389/feart.2019.00339.